Seismic Constraints on Core Structure and Dynamics

by

Thomas J. McSweeney

A dissertation submitted in partial fulfillment
of the requirements for the degree of

Doctor of Philosophy

University of Washington

1995

Approved by_____
Chairperson of the Supervisory Committee

Program Authorized
to Offer Degree_____

Date_____

In presenting this dissertation in partial fulfillment of the requirements for the Doctoral degree at the University of Washington, I agree that the Library shall make its copies freely available for inspection. I further agree that extensive copying of this dissertation is allowable only for scholarly purposes consistent with "fair use" as prescribed under U. S. Copyright Law. Requests for copying or reproduction of this dissertation may be referred to University Microfilms, 1490 Eisenhower Place, P.O. Box 975, Ann Arbor, MI 48109, to whom the author has granted "the right to reproduce and sell (a) copies of the manuscript in microfilm form and/or (b) printed copies of the manuscript made from microform."

Signature_____

Date_____

University of Washington

Abstract

Seismic Constraints on Core Structure and Dynamics

by Thomas J. McSweeney

Chairperson of the Supervisory Committee: Professor Kenneth C. Creager
Geophysics Program

We have picked the differential times of 2030 core-penetrating body waves from vertical-component, short period seismograms recorded by global and regional seismic networks. Using a cross-correlation technique, we have measured the difference in arrival times of 1730 P'_{BC}–P'_{DF} and P'_{AB}–P'_{DF} phase pairs. The P'_{DF} and P'_{BC} ray paths are very close to each other throughout the crust and mantle, so anomalous P'_{BC}–P'_{DF} times are most plausibly caused by core, rather than mantle, structure. While the P'_{AB}–P'_{DF} pair allows deeper imaging of the inner core, the P'_{AB} and P'_{DF} rays diverge in the lowermost mantle, making their times sensitive to aspherical structure of the lower mantle. P'_{BC}–P'_{DF} times for paths that are nearly parallel to the Earth's spin axis are consistently 2–4s larger than predicted by the radial earth model PREM, while rays in other directions have a mean and standard deviation of -0.01 ± 0.5 s. P'_{AB}–P'_{DF} times show a similar pattern, with residuals of 3–6s observed for rays nearly parallel to the spin axis and 0.05 ± 1.0 s for rays not near the spin axis. These observations lead to the robust conclusion that the inner core is strongly anisotropic. A simple model of hexagonally symmetric anisotropy aligned with the spin axis explains 54% of the variance in our observations. The symmetry direction which best fits the data and explains 59% of the variance is at 75°N, 170°E. This anisotropy is most likely due to preferrential alignment crystals within the inner core. Several alignment mechanisms have been proposed, and we propose several new ones. The only mechanisms which can explain the both the symmetry of the anisotropy with respect to the spin axis and the variation with depth are related to the existence of a strong toroidal magnetic field.

Thus, inner-core anisotropy may place constraints on models of the geodynamo. We have also used 1160 observations of P'_{AB}–P'_{BC} and P'_{AB}–P'_{DF} residuals to construct a model of the velocity structure of the Earth's D" region. Since the P'_{AB} ray is, on average, three times more sensitive to structure in the D" region than either the P'_{BC} or P'_{DF} rays, these residuals are most plausibly explained by the effects of structure near the interaction points of the P'_{AB} ray with the CMB. Using a stochastic inversion scheme, we have constructed a long-wavelength laterally heterogeneous model of the lowermost mantle. The resulting model explains nearly 50% of the variance in these residuals with only 32 degrees of freedom. In this model, there is significant long-wavelength structure in D", with peak to peak velocity perturbations (with respect to PREM) of ~3%. Finally, we compare predictions of the PREM model to the observations presented here. There are significant and systematic failures of PREM's fit to the differential travel time data presented here, indicating that the PREM model should be modified either in the D" region, the deep inner core, or both.

Table Of Contents

List of Figures

List of Tables

Acknowledgments

I would like to thank M. Brown, P. Shearer and G. Masters for helpful discussions, and S. Karato, P. Shearer, X. Song, L. Stixrude, and J. Tromp for sending us preprints of their papers. This study was made possible by the diligent efforts of many people who operate and distribute data from the Global Seismic Network (IRIS), Global Digital Seismic Network (distributed by the NEIC on CDROM), Alaska Seismic Network, and the Northern California Network (CALNET). H. Benz provided the CALNET data, while C. Rowe, and D. Christensen provided the ASN data. Rick Benson and Tim Ahern provided countless hours of help getting the FARM data in the right place at the right time. This work was supported by NSF.

Dedication

To my family, without whom this would have not been possible, and to Adriane, for putting up with my weird hours, long days and nights away from home, proofreading and checking my english, and providing the support and encouragement when things just wouldn't go my way.

Chapter 1: Introduction

1.1 Purpose of This Study

In this study, we will show that the models for the generation of the Earth's internal magnetic field through a geodynamo are constrained by current models of seismic anisotropy within the Earth's inner core. These models place constraints on the symmetry of the geodynamo and on the relative strength of the poloidal and toriodal components of the resulting internal magnetic field. For example, we suggest here that the Earth's magnetic field is a strong field rather than a weak field (the meaning of these terms is discussed in section 2.6) and that the toroidal component to this field is axisymmetric. This places a limit on the types of models that can be used to represent the process that generates the Earth's magnetic field. Since the geodynamo is the result of fluid motions in the liquid outer core of the Earth, these observations should also place constraints on models for convection in the outer core and, consequently, on models for the generation and transport of heat from the core to the mantle.

We will also show that the variations in the differential travel times of PKP phases place limits on the scale of P-wave velocity variations in the D" region of the Earth, thereby placing indirect constraints on current efforts to model mantle geodynamics. Measurements of the travel times and differential travel times of core body-waves (specifically PKP phases) constrain the scale and magnitude of CMB (Core-Mantle Boundary) P-wave velocity variations. When these velocity variations are compared with laboratory measurements of seismic wavespeeds of materials at CMB pressures and temperatures, one can infer the variations in parameters such as temperature, density, and composition. It is important to understand the magnitude and scale of variations in these parameters in order to model heat transport via conduction across the CMB and convection through the mantle.

The theme that we will be returning to again and again in this study is that seismic observations, when combined with laboratory measurements of Earth materials at high pres-

sures and temperatures, place important constraints on models of processes as widely varying as the geodynamo, core convection, heat transport from the core to the mantle, and on the geodynamics of the Earth's deep interior. While this has always been the case, current advances in seismic instrumentation, coverage by global and local networks, and availability of large datasets are making these sorts of constraints much more reliable and consistent than they have ever been in the past.

1.2 The Earth's Deep Interior

Structurally, seismologists typically divide the Earth into five major regions based on the variations in P and S velocities with depth: the crust, the upper mantle (which includes the transition zone), the lower mantle, the outer core, and the inner core. The crust and uppermost mantle (which both move together in plate tectonic motions) are often referred to jointly as the lithosphere. The lower boundary of the lithosphere is marked (in many places) by a low velocity zone (often referred to as the asthenosphere). The lithosphere acts as an upper boundary layer to mantle convection, since heat transport through this layer is predominantly conductive. The boundary between the upper and lower mantle is marked by changes in P and S velocities that are currently thought to be the result of a phase change in the major constituent of the mantle, olivine, at a depth of 660 km. The mode of heat transport throughout the mantle is thought to be convective, but there is presently a great deal of controversy as to whether the boundary at 660 km acts as a boundary to mantle convection. If so, then the upper and lower mantle must convect separately, otherwise the entire mantle convects as a single layer, with resultant mixing occurring between the upper and lower mantle. This question has important implications for the process of plate tectonics and the thermal state of the mantle as a whole. Regardless of the answer to this question of whole mantle or layered convection, the convection of the underlying mantle is intimately tied to the process of plate tectonics that is occurring at the surface of the Earth.

Beginning at a depth of ~2900km (a radius of ~3480km), the character of the Earth's interior changes dramatically. The top of this region of the Earth is marked by a change from the solid mantle to the liquid outer core. Initially it was thought that this liquid (outer)

core extended continuously to the center of the Earth. However, when P-wave arrivals where found in the shadow zone created by the low-velocity zone of the outer core [*Lehman*, 1936], a final region of the earth was proposed, a solid inner core with a radius of ~1225km. "Proof" that the inner core was solid, however, did not exist until much more recently, when it was found that the "best-fitting" models of the Earth's the normal modes had a non-zero shear modulus in the inner core [*Dziewonski and Gilbert*, 1972]. The detailed structure of the core, as determined by seismologists, will be discussed further in section 1.3.

In addition to defining regions of the Earth's interior based on seismic properties (above) the Earth can also be divided based on the composition of its interior. However, in and of itself, the study of the seismic properties of the Earth's core cannot determine its composition. The basic observations that seismology contributes to studies of the Earth's deep interior are the variations of P and S wave velocities (in body wave studies) or the density, shear modulus, and bulk modulus (in normal mode studies) either radially or in three dimensions. Experiments in wave propagation show that, for a given material, seismic velocities are dependent on both the density and mean atomic number of the elements that make up the material [*Poirier*, 1991]. Unfortunately for earth scientists, nearly all common rocks have similar mean atomic weights (from 21 to 22), so seismology alone cannot tell us the composition of the Earth's interior. To accomplish this, a combination of seismology and laboratory experiments in the high-pressure, high-temperature properties of materials must be used. Two techniques are commonly used to estimate the properties of materials at core pressures and temperatures: (1) shock-wave experiments that utilize explosives to generate a shock wave in a sample and measure the speed of the shock wave as it propagates through the sample at high temperatures and pressures, and (2) the diamond anvil cell, where the pressures are generated statically by pressing a small sample between two diamonds. High temperatures are commonly created by laser heating.

From laboratory measurements of seismic properties at high pressures and temperatures of materials with various compositions, measurements of compositions of mantle in-

clusions in crustal rocks, and measurements of the solar abundances of elements, it is thought that the mantle is composed primarily of iron and magnesium silicates. Based on differences between the abundances of elements hypothesized to make up the Earth's crust and mantle and observed solar abundances of elements, it is commonly accepted that the Earth's core is probably mostly composed of iron. Early models of the Earth's internal composition also allowed for the fact that the core might not be pure iron, but may, in fact contain some nickel, another element that is depleted in the Earth's crust and mantle relative to observed solar abundances. Unfortunately, when measurements were made in the laboratory, neither a pure Fe core nor a Ni-Fe core gave pressure-density curves at core pressures and temperatures that could satisfy the pressure-density curves obtained through seismic observations. An element lighter than Ni that can combine with Fe at core temperatures and pressures was needed.

Several alternative elements have been proposed to a Ni-Fe core composition in an effort to account for this difference between predicted and observed pressure-density curves. One possibility is sulphur [*Murthy and Hall*, 1970], which is also depleted relative to solar abundances. Several authors have studied this possibility using both shock wave experiments [*Ahrens*, 1979; *Brown et al.*, 1984] and static, high pressure experiments [*Kraft et al.*, 1982]. In all of these studies it was found that about 10 wt.% S in the outer core would be enough to account for the differences between the observed pressure-density curves and those predicted for a pure Fe core. A second alternative [*Anderson et al.*, 1989; *Jeanloz and Ahrens*, 1980; *Knittle and Jeanloz*, 1986; *Ringwood*, 1978] is oxygen. While O is a possibility, it is only able to alloy with Fe at high pressures, while S could have alloyed with Fe at much lower pressures (perhaps when both elements were present in the early Earth, before differentiation and subsequent core formation). This leads to difficulties only if one believes that the material that is now in the core formed at relatively low pressures (or shallow depths), which has been suggested by some authors in their models of differentiation of the Earth into a chemically distinct core and mantle. A third possibility is that potassium alloyed with iron in the Earth's core [*Hall and Murthy*, 1971; *Lewis*, 1971]. This possibility

has interesting implications for the thermal history of the Earth, since the presence of ^{40}K in the Earth's core would provide an internal energy source to drive both the geodynamo and mantle convection. However, disagreement between observed pressure-density curves in the Earth and those measured in shock wave experiments for $KFeS_2$ at core pressures [*Somerville and Ahrens*, 1980] suggest that there are no appreciable amounts of K in the core.

Compositionally, the core can also be differentiated into an inner and outer core. While the compositional change across the inner-core boundary is not thought to be nearly as dramatic as the compositional change across the CMB, a change is thought to exist. Comparison of seismically determined pressure-density curves with those determined in shock wave experiments show that the inner core, like the outer core, is not pure Fe, but is instead a mixture of Fe with some other light element. These high pressure experiments show that 3-7 wt.% S is required to match the seismically determined pressure-density curves [*Jephcoat and Olson*, 1987] and density contrast at the inner-core boundary (ICB). The presence or absence of such a light element as an alloy with Fe in the inner core has important implications for the source of energy for the geodynamo, since one of the proposed sources of energy is compositionally induced convection in the outer core. If the inner core were pure Fe and the outer core an alloy of Fe and S, then the crystallization of Fe from the outer core to form the inner core would set up a density imbalance that could drive convection in the outer core. If there is S in the inner core, this source of energy would be less than if the inner core were pure Fe, and it may not be sufficient to drive the geodynamo. In this case, another source of energy (such as thermal energy) may be necessary to drive core convection. A second important implication of the presence of S in the outer or inner core is that many present models of the temperature distributions in the core are based on the melting points of Fe at high pressures and temperatures. If there is S in the inner core, then the ICB may not represent a eutectic point in the iron phase diagram, but may instead be a chemical boundary. Such questions remain open to interpretation at the present time, and must be resolved before other questions such as the net heat flux through the CMB can be resolved.

Therefore, the answers to questions of the composition and structure of the Earth's core are important to the current efforts by earth scientists to understand such features of the Earth's interior as the geodynamo and the state of convection in the mantle. At the present time these questions cannot really be answered, partly due to uncertainties in the available seismic models of the core and partly due to the difficulties inherent in the laboratory measurements. To address the question of seismic models, we will turn next to what it is that seismologists know about the Earth's core.

1.3 Seismology and the study of the Earth's core

Compressional (α) and shear (β) wave speeds are estimated as a function of radius from observations of travel times of a variety of compressional (P) and shear (S) wave travel times. While these velocity variations may be of direct interest to seismologists for a number of reasons (such as locating earthquakes), those who are attempting to model processes within the Earth are also interested in parameters that are related to these velocities, such as density, composition, pressure, and temperature. To obtain density as a function of depth in the Earth's deep interior, seismologists use a relationship called the Adams-Williamson relationship, which relates the seismic parameter (ϕ) to the variation in density (ρ) as a function of depth by

$$\frac{d\rho}{dr} = \frac{-Gm\rho^2}{\kappa r^2} = \frac{-Gm\rho}{r^2\phi} \qquad 1\text{-}1$$

where G is the gravitational constant, r the radius, m the mass contained in the sphere of radius r, ρ is the density, κ is the bulk modulus and the seismic parameter (ϕ) is defined as

$$\phi = \frac{\kappa}{\rho} = \alpha^2 - \frac{4}{3}\beta^2 \qquad 1\text{-}2$$

This relationship is valid under the assumptions of chemical homogeneity and hydrostatic pressure and assumes that the temperature gradient within the region of interest is adiabatic (all of which are considered to be valid assumptions in the Earth's deep interior if the crust, uppermost mantle, transition zone, lower mantle, outer core and inner core are considered

separately). Given this relationship and variations in $\alpha(r)$ and $\beta(r)$ earth scientists can determine $\rho(r)$ by numerically integrating equation 1-1. Once density is known as a function of depth, several other parameters can be determined. First, the bulk modulus (κ) and shear modulus (μ) as a function of depth can both be determined using a combination of the shear wave velocity ($\beta = \sqrt{\mu/\rho}$) and the compressional wave velocity ($\alpha = \sqrt{(\kappa + [4/3]\mu)/\rho}$) and as a function of depth. Second, local gravitational acceleration, $g(r)$, can be determined once the density is known as a function of depth. Finally, once both $g(r)$ and $\rho(r)$ are known, the pressure, $p(r)$, can be determined as a function of depth (if the assumption of hydrostatic pressure can be made). Determination of both $\rho(r)$ and $p(r)$ accurately is important if one is to attempt to use laboratory analyses (like shock-wave and diamond-anvil experiments) to relate seismic observations to earth composition and structure.

But there are problems with the inversion of travel times to determine the radial variations in P and S wave velocities. The biggest is the problem that is encountered when there is a "low-velocity zone" (or LVZ) within the Earth. In this situation, the velocity decreases, rather than increases, as a function of depth at a rate greater than v/r. The result is a "shadow zone" where there are no arrivals for a distance range whose size and location depend on the depth, thickness and velocity profile of the LVZ. A direct result of a shadow zone is that the inversion technique that is used to determine $\alpha(r)$ and $\beta(r)$ breaks down, and the solutions are not unique. In fact, it was just such an observation of a "shadow zone" in direct P-wave arrivals (from 105° to 143° in distance) that led to the proposal the there was a third major region within the Earth (the core). The fact that there were no S-waves observed beyond the equivalent SH (horizontally polarized S wave) "shadow zone" was used as support for the concept that the Earth's core was a liquid, rather than a solid (in a liquid the shear modulus, μ, goes to zero and, as a result, it cannot transmit shear waves). This P-wave "shadow-zone" was also critical in discovering the existence of the deepest major region in the Earth, the inner core. The existence of the inner core was proposed when P waves were observed in this "shadow zone" [*Lehman*, 1936]. The existence of these observations ($PK-P_{CD}$ and PKP_{DF} phases) suggested that there was a sudden increase in velocity within the core. Bullen [1953] proposed a simple argument that the inner core was solid based on the

size of the velocity jump at the inner core boundary. There is a jump of ~6% in P wave velocity across the ICB (or ~13% in α^2). If the entire core is liquid, then the P wave velocity is given by the acoustic wave velocity $\alpha = \sqrt{\kappa/\rho}$. This suggests that as one descends across the ICB there is either a 13% decrease in density or a 13% increase in the bulk modulus (or some combination of both). Density cannot decrease with depth in the core if it is a liquid, since it would create a gravitationally unstable situation, which would certainly be removed by the effects of convection. In addition, from his estimates of bulk modulus throughout the mantle and core, Bullen found that in the deep Earth there was very little variation in either bulk modulus or the change in bulk modulus with pressure throughout the mantle and core, even across the core-mantle boundary (if the D" region is ignored). This suggested that at the temperatures and pressures of the Earth's deep interior, bulk modulus doesn't change much at all. Instead, Bullen proposed, it is more likely that the inner core has a non-zero rigidity, in which case the P-wave velocity is replaced by

$$\alpha = \sqrt{\frac{\kappa + (4/3)\mu}{\rho}} \qquad 1\text{-}3$$

and the 6% velocity increase can be explained simply by an increase in the shear modulus to a non-zero value. If density increases as well (as is currently thought to happen at the ICB), this increase in the shear modulus would have to be substantially larger.

The average P-wave structure in the outer core and the average radius and ellipticity of the core-mantle boundary are constrained quite strongly by studies of PcP, ScS, P_{diff}, S_{diff}, PKP, and SmKS phases [*Masters and Shearer*, 1990]. For example, Engdahl and Johnson [1974], used PcP at nearly vertical incidence to obtain a radius for the outer core of 3485 ± 3 km, which is in close agreement with present day estimates. In a similar fashion, Engdahl et al. [1974] and Bolt [1982] used PKiKP times to estimate the radius of the inner core boundary (or ICB). Their ICB radii were 1225 ± 5 km and 1216 ± 2 km respectively. Souriau and Souraiu [1989], on the other hand, used PKiKP-PcP differential travel times at nearly normal angles of incidence to measure the ellipticity of the inner core. They found

that the inner core was very nearly in rotational equilibrium and that the radius of the inner core was, on average, about 1216 ± 3 km. Similarly, many attempts have been made to determine the S-wave velocity structure of the inner core. Although claims have been made that PKJKP, a body wave phase that is an S wave when it traverses the inner core, has been identified in seismograms [*Julian*, 1972], this phase is likely to be so small that attempts at observation, even using array data, are unlikely to succeed [*Doornbos*, 1974]. The strongest support for the S-wave velocity structure in the inner core, to date, comes from observations of normal modes of core-sensitive phases. The best fit models for these modes all include an inner core with non-zero rigidity [*Dziewonski and Gilbert*, 1972]. While early measurements of inner-core-sensitive modes were found to be a consequence of anomalous splitting of nearby modes which have most of their energy in the outer core, about 50 modes that have been reliably measured are sensitive to S-wave structure in the inner core. The best fitting models to this data have β values of about 3.45km/sec [*Masters*, 1991].

Since a great deal of information about the deep interior of the Earth has been determined using the normal modes of the Earth, they deserve special mention. In the last 30 years, great strides have been made in trying to understand the free-oscillation spectrum of the Earth's normal modes. After a large earthquake, the Earth rings "like a bell" with seismic energy, and the frequencies of these modes of vibration of the Earth can be used to determine the interior structure of the Earth. Unfortunately, the periods of the modes of oscillation that are observed that are sensitive to structure in the deep interior of the Earth are on the order of hundreds of seconds. As a result these observations are able to place constraints on the variations of properties in the Earth's deep interior that have spatial scales from several hundred to a thousand kilometers. In utilizing these observations to determine mantle structure, seismologists typically use them in inverting for mantle P and S wave velocity structure by simultaneously inverting observations of both mode eigenspectra and long-period body wave travel-times for Earth structure. There are two major advantages of normal mode observations over body wave observations. First, the quantities that are determined by the mode observations are the density, bulk modulus and shear modulus of the

material, properties that can only be determined with a great deal of effort using body waves (see the above discussion on the Adams-Williamson relationship). Second, the modes physically average large regions of the Earth's deep interior, reducing the problems related to spatial aliasing that are so prevalent in inversions of body-wave travel times for deep Earth structure. Unfortunately, until quite recently, digital recordings of large, deep earthquakes have been essentially non-existent. Large earthquakes are necessary to excite the normal modes of the Earth above ambient noise levels. Deep sources preferentially excite modes containing energy in the deepest parts of the Earth, including the core. The two largest earthquakes of this century (The Great Alaskan Earthquake in 1964 and the Chilean Earthquake in 1960) were both prior to the first deployment of a worldwide network of digital seismographs (the International Deployment of Accelerometers, or IDA), and the only data available for these earthquakes are analog recordings from long period instruments of the WWSSN. Since the development of broadband instrumentation, there have been no great earthquakes, and no large (i.e. $M_w > 8.0$) deep earthquakes until just last year. Last year, a moment magnitude 8.3 earthquake at a depth of 600km occurred under northern Bolivia. The modes that were excited (many of which had never been observed) are still being studied in order to determine the structure of the Earth's core.

The existence of high quality digital data (which has been available since the late 1960's from the IDA network), greatly simplifies the procedure of determining the mode eigenspectra and makes it possible to include a larger number of accurately determine mode observations in a given study. Similarly, while it is possible to study the Earth's deep interior using hand picked travel times from a few analog recordings of body waves, it is much simpler to make large numbers of travel time "picks" of body wave phases using continuous recordings of digital data. With the development of the modern, positive feedback, broadband seismometers (which have a much higher dynamic range than previous instruments) and the installation of the Global Seismic Network (GSN) by the Incorporated Research Institutions for Seismology (IRIS) and the Federation of Digital Seismic Networks (FDSN, of which IRIS is one part), comprehensive seismic studies of the Earth's deep in-

terior by both body wave studies and normal mode studies are now possible. All of the data from these instruments are recorded continuously and are archived in one central location (the IRIS Data Management Center, or IRIS DMC, in Seattle) in a common format (Standard for the Exchange of Earthquake Data, or SEED). Rather than requiring the investigator to travel to the archive to extract data from it, the data are readily accessible by either customized requests to the IRIS DMC or anonymous ftp from the archive on the Internet or the World Wide Web. As a result, it is becoming much easier to incorporate large numbers of globally collected observations of body waves and/or normal modes into a study of the Earth's deep interior. This has already had a large impact on the types of studies that can be undertaken (even though the time span covered by this dataset is currently rather small), and the picture is only improving as time goes by (both in terms of quantity of data and station coverage). Without global networks such as these, this study (and the results it contains) would not have become a reality.

In this study, we analyze data from two regional networks and two global networks. The regional network data were taken from a set of 5 events from the South Atlantic and Southern Indian ocean recorded at the Alaska Seismic Network (ASN) and the CALNET array in Northern California. The global network data were waveforms from the Global Digital Seismic Network that were recorded from 1977-1987 and waveforms from the Global Seismic Network that were recorded from 1988-1994. The GSN replaced (and in many cases inherited stations from) the GDSN in the late 1980's. The earliest (1977-1979) and latest (1988-1994) datasets were obtained from the IRIS Fast Archive Recovery Method (FARM) data, while the data from 1980-1987 were obtained from the dataset distributed by the National Earthquake Information Center (NEIC) on CDROMs. We have picked 300 P'_{AB}–P'_{BC}, 765 P'_{BC}–P'_{DF} and 965 P'_{AB}–P'_{DF} differential travel times in order to image the structure of the CMB and the inner core. The global networks provide data that are useful for obtaining the large-scale lateral variations in the structure of the CMB and inner core, which the regional networks provide data to focus on special areas of interest.

This study divides itself quite naturally into two distinct parts. In Chapter 2 we estimate

the seismic anisotropy in the Earth's inner core. We will also discuss the implications that this model of inner core anisotropy has for current efforts to model the generation of the Earth's magnetic field using various types of geodynamos. Seismology has important constraints to make on the models available for this process. In Chapter 3 we will use these observations to constrain the scale and the magnitude of heterogeneity in P-wave velocity structure in the D" region of the Earth (just above the core-mantle boundary). Chapter 4 describes additional experiments for which these data will be useful. Finally, the Appendix discusses our observations in relation to the radial earth model PREM.

Chapter 2: Inner-core seismic anisotropy and implications for the geodynamo

2.1 Introduction

The primary goals of this paper are to investigate seismic anisotropy of the Earth's inner core and the possible mechanisms underlying the anisotropy. The most plausible mechanisms seem to have important consequences for the origin and evolution of the earth's magnetic field. There are many partial differential equations that must be simultaneously solved to obtain a viable solution for the origin of the Earth's magnetic field [*Merrill and McFadden*, 1983]. These equations are often coupled to each other and include non-linearities. Hence, no complete solution to the geodynamo problem exists. Here we show how seismology can be used to reduce the variables involved and to eliminate some types of dynamo models from the list of viable options. Moreover, the variation in anisotropy with depth may provide valuable information on the evolution of the Earth's magnetic field.

It was a nice piece of detective work that led Morelli et al. [1986] and Woodhouse et al. [1986] to postulate that the inner core is strongly anisotropic. This inference was based on anomalously split normal-mode eigenfrequencies, first observed by Masters and Gilbert [1981] and Ritzwoller et al. [1986], and on latitudinal variation of travel-time residuals of P'_{DF} phases. Similar travel-time anomalies were observed by Poupinet et al. [1983], but interpreted as topography of the inner-core boundary. Though the existence and degree of anisotropy in the inner core was vigorously debated during the late 1980's, recent analyses of three different data sets have lead to the consensus among seismologists that the inner core is anisotropic with an amplitude of about 3% and a symmetry direction nearly parallel to the Earth's Spin axis. The three data sets are hand-picked [*Creager and Jordan*, 1986; *Song and Helmberger*, 1993a; *Vinnik et al.*, 1994] PKIKP travel times, International Seismological Centre (ISC) [*Shearer*, 1994] PKIKP travel times, and anomalous splitting of normal-mode eigenfrequencies [*Tromp*, 1993].

Before presenting the results of the body wave analyses of inner-core structure, we describe the ray geometry. The phase naming convention results from labeling the end points of a travel-time curve for core-penetrating compressional waves (Figure 2-1). The P'_{AB} and P'_{BC} branches, sometimes called simply PKP, represent rays that turn in the outer core (Figure 2-1b). The existence of two distinct phases is the result of the outer core being a low velocity zone. The P'_{AB} phase has "touched a caustic" which causes a 90° phase advance and a distortion of the waveform [*Choy and Richards*, 1975]. This distortion can cause bias in travel-time picks from analog seismograms, but can be corrected using Hilbert Transforms of digital records (Figure 2-2). Over the distance range of interest in this paper, P'_{CD}, or PKiKP, reflects off the inner-core boundary, has relatively low amplitude, and is typically in the coda of either the P'_{DF} or P'_{BC} branch. P'_{DF}, or PKIKP, turns in the inner core and is the phase used to infer inner-core structure. This phase is predicted to be the first arrival, so it is often the most reliably picked phase. However, in the distance range from about 130 to 145°, energy scattered off the core-mantle boundary (CMB), can arrive earlier than P'_{DF} complicating its interpretation [*Haddon and Cleary*, 1974]. From 147° to about 155° P'_{BC} arrives a few to ten seconds after P'_{DF}, but is larger in amplitude, making it relatively simple to pick both phases. P'_{BC} bottoms at the inner-core boundary at a distance of about 152° and diffracts around the inner core at greater distances, causing it to decay rapidly in amplitude at greater distances. On the other hand P'_{AB} has the same minimum distance, but continues to nearly 180° (Figure 2-1a).

Estimation of inner-core structure is complicated by the fact that ray paths which sample the inner core also sample the rest of the Earth above. In the epicentral distance range 150 to 180° P'_{DF} rays spend 11% to 18% of their time in the inner core. Three approaches have been adopted to address this problem. One is to "correct" the observed travel-time residuals of P'_{DF} by relocating earthquakes, and applying travel-time corrections for models of large-scale aspherical mantle structure, and station corrections for near-receiver structure [*Su and Dziewonski*, 1994]. A second is to consider a statistical approach [*Shearer*,

(a)

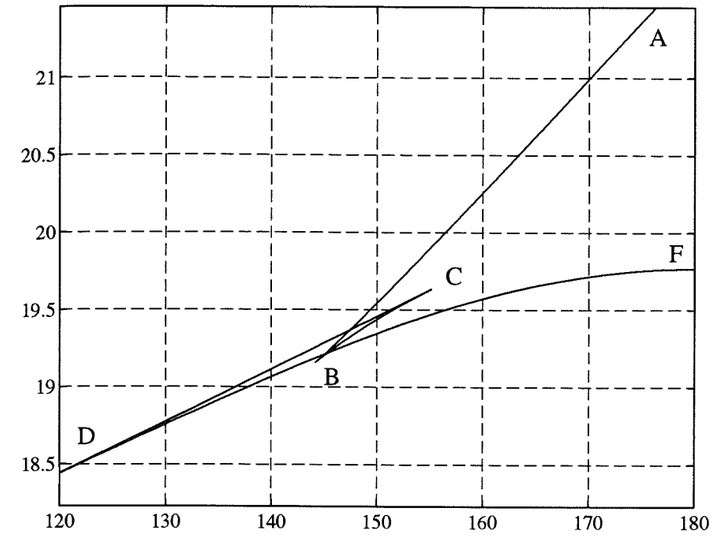

(b)

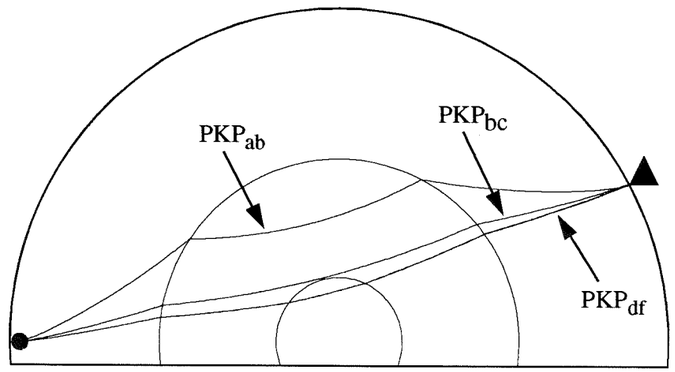

Figure 2-1: (a) Travel-Time Curve for an earthquake at 200km depth. The endpoints of the "branches" of the travel-time curve are labeled A, B, C, D, and F, as discussed in the text. (b) Ray Geometry for an earthquake at the same depth and an earthquake-station distance of 152 degrees. The earthquake is represented by the circle, the station by the inverted triangle and the rays used in this study are labeled PKP_{AB}, PKP_{BC}, and PKP_{DF}, respectively

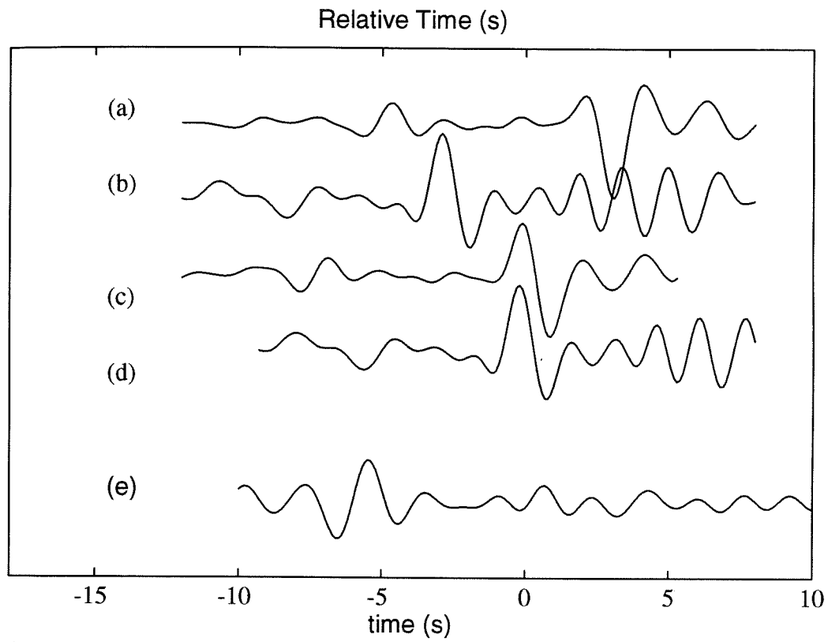

Figure 2-2: Vertical component, short-period seismogram from station WRH of the Alaska Seismic Network showing the P'_{AB} (a) and P'_{DF} (b) phases aligned with respect to predicted times based on the radial model PREM. The P'_{AB} phase has been inverse Hilbert Transformed and aligned with the P'_{DF} phase (c and d) by using the lag time in the peak of their cross correlogram (e). All P'_{AB} minus P'_{DF} residuals were picked using this method, though we used shorter time windows. This seismogram is also displayed in Figure 2-4.

1994]. For example, consider all rays sampling the inner core in a given direction. Calculate a robust average of these times. If these rays sample significantly different parts of the upper layers of the Earth, this averaging scheme will reduce their effects relative to the effects of inner-core anisotropy.

A third approach, which we use in this report, is to analyze differential travel times, i.e. the time differences between pairs of phases. If both rays pass through the same velocity anomaly they will both be delayed (or advanced) by the same amount and the differential time will be unaffected. The advantage of this technique for a phase pair such as P'_{BC}–P'_{DF} is illustrated by a ray diagram (Figure 2-1b). The ray paths remain within about 300km of each other throughout the crust and mantle. Differential travel-time anomalies are primarily caused by structure in the inner core or innermost outer core, because that is the only region where these two rays sample distinctly different areas of the Earth (Figure 2-1b). Also, the take-off angles at the source are nearly the same, so earthquake mislocations will have a small effect on the differential times. Unfortunately, P'_{BC} does not extend beyond about 155°. At this distance P'_{DF} only penetrates 300km into the inner core. In order to look deeper into the inner core, we analyze the phase pair P'_{AB}–P'_{DF}. The take-off angles differ by as much as 11° at a distance of 165°, so this phase pair is more sensitive to bias owing to earthquake mislocation [*Helffrich and Sacks*, 1994]. These phases deviate by as much as 2800km near the base of the mantle, and P'_{AB} transits D" at near grazing angles so this differential time pair is sensitive to lateral variations in deep mantle structure as well as to inner-core structure. In Chapter 3, we will be using this sensitivity of the P'_{AB} phase to deep mantle structure to study this region of the Earth. For now, however, we must realize (when making inferences regarding inner-core structure) that this phase pair may be effected by deep mantle structure, so our interpretations of the results of this phase pair must be made cautiously. In modeling the P'_{AB}–P'_{DF} and P'_{BC}–P'_{DF} differential travel times with inner core anisotropy (see section 2.4) we will be giving the P'_{BC}–P'_{DF} differential travel times a greater weight in the inversion for exactly this reason.

Morelli et al. [1986] found that P'_{DF} travel-time residuals calculated from ISC observations at epicentral distances greater than 170° showed a consistent pattern with paths parallel to the Earth's spin axis about 2s faster than equatorial paths. These observations were explained with a simple model of inner-core anisotropy with polar paths 3.2% faster than equatorial paths at the inner-core boundary. The anisotropy decayed as the square of radius. Subsequent analyses of ISC P'_{DF} times suggested that the anisotropy was limited to about 1% in amplitude [*Shearer and Toy*, 1991; *Shearer et al.*, 1988], however, travel-time residual in excess of 1.5s were considered to be reading errors and were discarded. Creager [1992] pointed out that the ISC data set exhibits consistent 2 to 3 second differential (P'_{BC}–P'_{DF}) residuals for polar paths. Upon reanalysis of the ISC data using a boot-strap method on times binned by turning depth and ray direction, Shearer [1994] found consistent P'_{DF} residuals as large as 5s for rays traveling nearly parallel to the Earth's spin axis. This suggests that the ISC data are consistent with large-amplitude (3%) anisotropy.

Shearer and Toy [1991] recognized the importance of P'_{BC}–P'_{DF} differential times and picked them from digital data recorded by the Global Digital Seismic Network (GDSN). Unfortunately, however, none of the picks corresponded to pole parallel paths. Creager [1992] did the same thing, but found 20 seismograms corresponding to pole parallel paths. These observations were the basis of his model for inner-core anisotropy in which the pole-parallel direction is 3.5% faster than paths normal to the spin axis. Song and Helmberger [1993a] improved the geographic sampling of the inner core at pole-parallel directions by analyzing differential times (P'_{BC}–P'_{DF}) from digital and analog records. Their observations are consistent with 3% anisotropy.

Recent efforts, including this paper, have focused on the depth variation of inner-core anisotropy. P'_{DF} residuals calculated from the ISC picks at distances greater than 160° reach values as large as 5s [*Shearer*, 1994] and P'_{AB}–P'_{DF} residuals are 3-6s at distances greater than 170° [*Vinnik et al.*, 1994]. In this report, we interpret similar size residuals for pole parallel paths, and suggest that the inner-core anisotropy reaches 4% at 500km deep

into the inner core.

The third, and final, source of data used to constrain inner-core structure is observations of anomalously split normal modes. The Earth responds to very large earthquakes by resonating at a set of distinct eigenfrequencies. In a spherically symmetric planet, these eigenfrequencies would be degenerate, but aspherical structure causes observable splitting of the eigenfrequencies (similar to the loss of a distinct tone in an imperfect bell). Modes that are sensitive to the Earth's core are observed to be split more than expected owing to rotation and ellipticity of figure [*Masters and Gilbert*, 1981; *Ritzwoller et al.*, 1986]. Woodhouse et al. [1986] proposed that the split modes were caused by anisotropy of the inner core. As data and analysis techniques improved, this group argued repeatedly that the modes were consistent with inner-core anisotropy, characterized by the fast direction being parallel to the spin axis, but that the modes did not have sufficient resolution to constrain the details [*Giardini et al.*, 1987; *Li et al.*, 1991; *Woodhouse et al.*, 1986]. Widmer et al. [1992] nearly double the number of observed core-sensitive split modes and argued that many of the modes which were strongly split contained less than 2% of their energy in the inner core. Thus, the inner core is an unlikely place to look for the structure causing the splitting. Recently, however, Tromp [1993] generated a model of cylindrically axisymmetric inner-core anisotropy that fits not only these anomalously split modes, but also Creager's [1992] observations of differential travel times of PKP and PKIKP phases.

In this study, we more than triple the number of published high-quality hand-picked P'_{BC}–P'_{DF} times for ray paths nearly parallel to the Earth's spin axis, while increasing the number of deeply penetrating P'_{AB}–P'_{DF} times by an order of magnitude. Our preferred model exhibits near axi-symmetric anisotropy with the fast direction parallel to the spin axis. The level of anisotropy is greater than 3% at a depth of 150km into the inner core, increasing to about 4% at a depth of 500km into the inner core. Below this, the level of anisotropy appears to decrease to a depth of 800 km. Resolution at shallower and greater depths is weak. This suggests that the anisotropy in the inner core does not decay with depth as has been proposed in previous studies of both body waves and normal mode splitting. In

fact, it appears to increase to a maximum value at a depth of about 500km into the inner core, then decrease with decreasing radius. The nearly cylindrical symmetry of this anisotropy with respect to the rotation axis places a strong constraint on mechanisms that could give rise to this anisotropy. Even if convection (creep) in the inner core occurs and causes crystal alignment, itself a controversial issue [*Karato*, 1993], its speed would certainly be so slow that Coriolis force would be negligible. Hence, it is difficult to see how convection processes could produce the observed symmetry in the inner core. Instead, it may be the time average of processes that act in the outer core, where the Coriolis force is not negligible, that somehow affect processes in the inner core, particularly near its boundary. This possibility is explored in section 2.7, where we link mechanisms for causing axi-symmetric seismic anisotropy to the diffusion of a time-averaged magnetic field with rotational symmetry across the inner core boundary.

2.2 Differential-Time Observations

We measured the differential travel times of P'_{AB} minus P'_{DF}, and P'_{BC} minus P'_{DF} from 40 globally distributed stations of the Global Digital Seismic Network (GDSN), 65 stations from the Alaska Seismic Network (ASN), operated jointly by the United States Geological Survey (USGS) and the University of Alaska, Fairbanks, 166 stations of CALNET regional array, which is operated by the USGS in northern California, and 118 stations of the Global Seismic Network (GSN), which is operated by the Incorporated Reseach Institutions for Seismology (IRIS) in cooperation with the other members of the Federation of Digital Seismic Networks (FDSN). Times were measured from the vertical component, short-period seismograms, which typically have a dominant period of about 1 second. In the case of the GSN data, the broad-band seismograms were converted to short-period seismograms by deconvolving the broad-band instrument response from the seismograms and reconvolving the standard DWWSSN short-period instrument response with the deconvolved data, while the short-period seismograms were left unchanged. If the same event-station pair had both a broad-band and short-period seismogram recorded by the GSN, the short-period seismogram was used rather than the broad-band seismogram. As a result the

GDSN, CALNET, ASN and GSN data can be used together in modelling deep earth structure.

The time difference between two phases on the same seismogram is estimated by selecting 5 to 15 second windows around each phase, and cross correlating the traces in pairs (Figure 2-2). P'_{AB} has touched a caustic which gives it a 90° phase shift with respect to the P'_{BC} and P'_{DF} phases. We correct for this by applying an inverse Hilbert Transform to the P'_{AB} waveform prior to cross-correlation. The differential time of each phase pair is estimated from the lag time of the highest peak in the cross correlogram. The quality of each differential time was assessed by evaluating the alignment of the two phases and the shape of the cross correlogram. Particular attention was paid to the alignment of the phases at their onset and to the similarity of the waveform shapes. We looked at about 10000 phase pairs in this manner. About 4000 had sufficient signal to noise ratios to estimate differential times. For this study, we interpret only the 1730 times for which we were 95% to 99% confident of no cycle skipping errors. Since the dominant period of the seismograms is typically about 1 second, reading errors of 1 second or more are rare. For each seismogram we determined the theoretical arrival times of all depth phases, such as pP'_{DF}, and rejected seismograms in which a depth phase could be misinterpreted as P'_{AB} or P'_{BC}. The seismographs used for the two regional arrays (CALNET and the ASN) are sensitive to higher frequencies than those used for the GDSN. To improve the stability of our measurements, we applied a 4 pole, low-pass Butterworth filter with a cutoff frequency of 2 Hz to the regional array data prior to analysis. No filtering was applied to the GDSN data.

Because the inner core has a low Q [*Bhattacharyya et al.*, 1993], the P'_{DF} phase is typically depleted in high frequencies. This is especially apparent in seismograms from deep Tonga earthquakes to station BCAO in Africa. For this source region and receiver the P'_{BC} phase often contains abundant high frequency energy, which is not present in P'_{DF}. Dispersion owing to attenuation will cause the travel times to be frequency dependent [*Aki and Richards*, 1980]. However, because of the narrow band nature of the seismograms we an-

alyzed, the dispersion caused by inner-core attenuation has only a subtle effect on our differential travel times. Assuming Q is not dependent on frequency, dispersion in seismic waves due to the low Q of the inner core, over the frequency ranges of the waveforms utilized in this study, should bias our observed differential travel times (P'_{AB}–P'_{DF} and P'_{BC}–P'_{DF}) by less than 0.1 second. Thus, we will not concern ourselves with this effect. However, if Q is strongly frequency dependent, dispersion can affect times by as much as 1s [*Cormier*, 1994]. This is much smaller than the 3–6s anomalies we observe, and would represent apparent inhomogeneity in seismic wave speeds, not the directional dependence we need to explain our observations.

Differential travel-time residuals are calculated with respect to the radial earth model PREM [*Dziewonski and Anderson*, 1981] by subtracting predicted differential times from observed differential times. These residuals are calculated as P'_{BC}–P'_{DF} or P'_{AB}–P'_{DF}, so that positive residuals correspond to a late P'_{BC} or P'_{AB} phase, or an early P'_{DF} phase (i.e. positive residuals correspond to high velocities in the inner core or low velocities along the P'_{BC} or P'_{AB} branch in the outer core). Times are corrected for the Earth's ellipticity [*Dziewonski and Gilbert*, 1976]. Source locations are taken from either the ISC (the catalog of the International Seismological Centre) or the PDE (the Preliminary Determination of Epicenters).

The most striking signal in these observations is the large positive differential-time residuals corresponding to ray paths that are nearly parallel to the Earth's spin axis at their bottoming points (open and solid diamonds in Figure 2-3a). These residuals increase systematically from 2 to 6 seconds as epicentral distance increases from 148 to 165° (as ray turning radii decrease from 1000 to 500 km). Beyond this distance range, these residuals decrease systematically from 6 seconds at 165° to 4 seconds at 170°.

GDSN: From the globally distributed stations of the GDSN, we picked 264 P'_{BC}–P'_{DF} and 244 P'_{AB}–P'_{DF} times with ξ>40. ξ is the angle between the P'_{DF} ray at its turning point and the spin axis of the Earth. Their mean values are 0.2 and 0.3s respectively, so our ob-

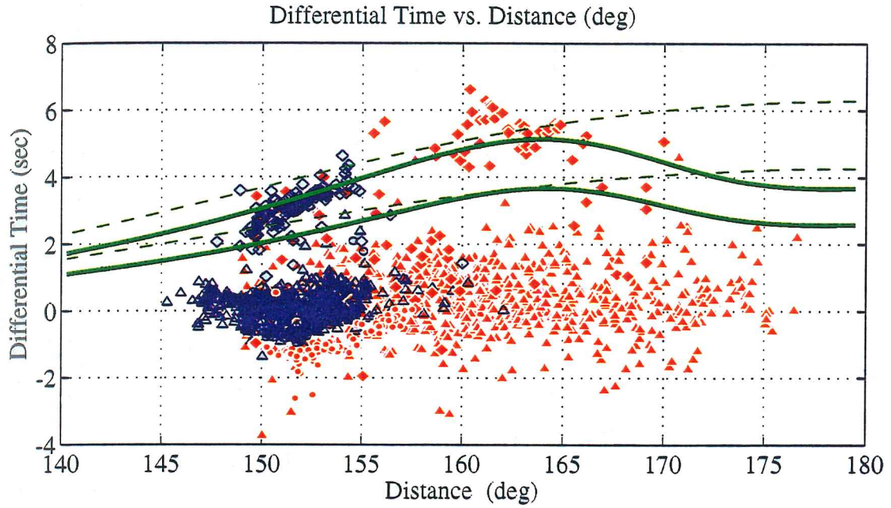

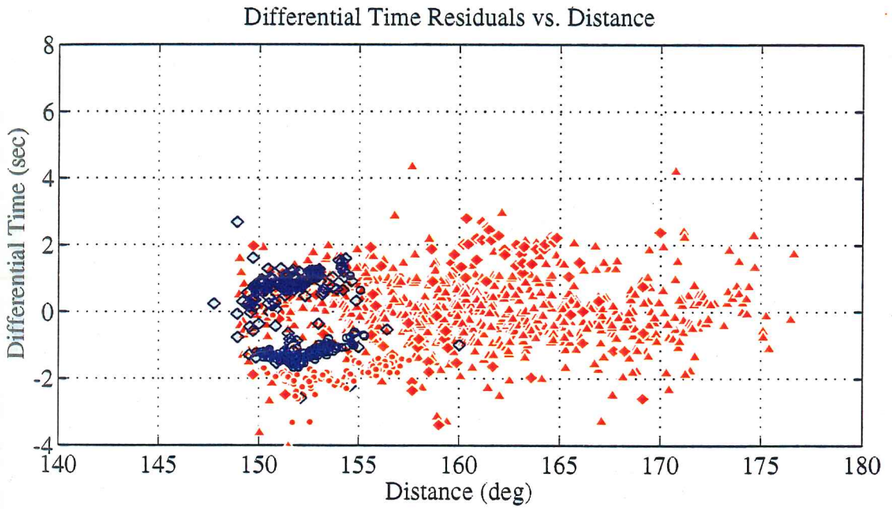

Figure 2-3: Differential travel-time residuals (P'_{BC}–P'_{DF} (blue) or P'_{AB}–P'_{DF} (red) with respect to PREM (a) and after correction for anisotropy model AXSYM (b) versus epicentral distance. Times separated into GDSN, FARM, and ASN data with $\xi > 40°$ (triangles), those with $\xi < 40°$(diamonds) and CALNET data (circles). Predicted times for our model (AXSYM, solid lines) and Creager's (1992) model (dashed lines) are shown for ray angles of $\xi = 20°$ and 30°.

servations are generally consistent with PREM. However, the standard deviation of the P'_{AB}–P'_{DF} times is 0.9 s, more than twice that of the P'_{BC}–P'_{DF} times (0.4 s). This difference is caused primarily by structure near the CMB (as discussed below), though there may be contributions from earthquake mislocations, slab structure, or other deep-mantle heterogeneity [*Helffrich and Sacks*, 1994].

Creager [1992] picked 20 P'_{BC}–P'_{DF} times which had ray angles less than 40° from the spin axis. These have a mean value of 2.9 s, 7 standard deviations away from the P'_{BC}–P'_{DF} times with ξ>40°. He used these observations to argue for anisotropy extending to a depth of at least 300km into the inner core with a magnitude of 3.5%. Fifteen of these picks were to station COL in central Alaska. The remaining five, as well as several picks by Song and Helmberger [1993a], provide a more uniform coverage of the globe and support the model of strong axisymmetric anisotropy.

FARM: From the stations of the GSN, we picked 619 P'_{BC}–P'_{DF} and 870 P'_{AB}–P'_{DF} times with ξ>40. Their mean values are -0.15 and 0.53s, respectively, so, as with the GDSN data our observations are generally consistent with PREM. The standard deviation of the P'_{AB}–P'_{DF} times is 1.04s, more than twice that of the P'_{BC}–P'_{DF} times (0.5s). As with the GDSN times, we feel this difference is caused primarily by structure near the CMB.

ASN: To test these models, we analyze data from five earthquakes (Table 2-1, page 25) to the ASN array, which contains about 100 stations in Alaska separated by as much as 1000 km. We picked 97 P'_{BC}–P'_{DF} times from events 2–4 (Table 2-1). Travel-time anomalies across this large aperture array from three events separated by up to 40km in depth and 250km in epicenter have a mean value of 3.2s and a standard deviation of only 0.5s. This result is consistent with the 2.9s average of P'_{BC}–P'_{DF} residuals observed by Creager (1992) at station COL in Fairbanks, Alaska for 15 events separated by 170km in depth and 500km in epicenter.

Table 2-1: Event List for ASN and CALNET Data

event no.	date	time	latitude(N)	longitude(E)	depth(km)
1	90/04/30	05:54:41.5	–54.310	1.250	10
2	91/12/27	04:05:58.2	–56.032	–25.266	10
3	91/12/28	00:52:10.1	–56.102	–24.614	10
4	91/06/15	01:13 21.4	–58.285	–24.183	52
5	93/03/29	06:57:19.5	–53.039	27.396	10

Most of the variation in the GDSN, FARM, and ASN observations is related to an epicentral distance trend (Figure 2-3a, open diamonds). When this trend is removed the standard deviation in the ASN times is reduced to only 0.2s. Note that the P'_{AB}–P'_{DF} residuals to these same stations (solid red diamonds at distances less than 158°) are consistent with this trend but show much more scatter. The scatter is likely due to contamination of the P'_{AB} branch by D" structure. The fact that both the P'_{AB}–P'_{DF} and P'_{BC}–P'_{DF} show similar trends provides further evidence that the anomalous structure lies along the P'_{DF} ray.

To look deeper into the inner core, we also analyzed P'_{AB}–P'_{DF} residuals at the ASN array for events 1–5 (Table 2-1). Of particular interest is event 1 in the South Atlantic Ocean recorded at a epicentral distances of 156 to 166°. This corresponds to ray turning radii from about 800 to 500 km. A record section of the 41 seismograms with the best signal to noise ratios is displayed in Figure 2-4. The observed differential times exceed the predicted differential times by 4 to 6.5 seconds with a mean and standard deviation of 5.4 ± 0.5 s. These extremely large residuals are consistently observed across the network, and many of the times can be picked without ambiguity. For example, Figure 2-2 shows the P'_{AB} and P'_{DF} waveforms for station WRH at a distance of 162°. Seismograms are displayed aligned relative to PREM (Figure 2-2a and b), and aligned using our cross-correla-

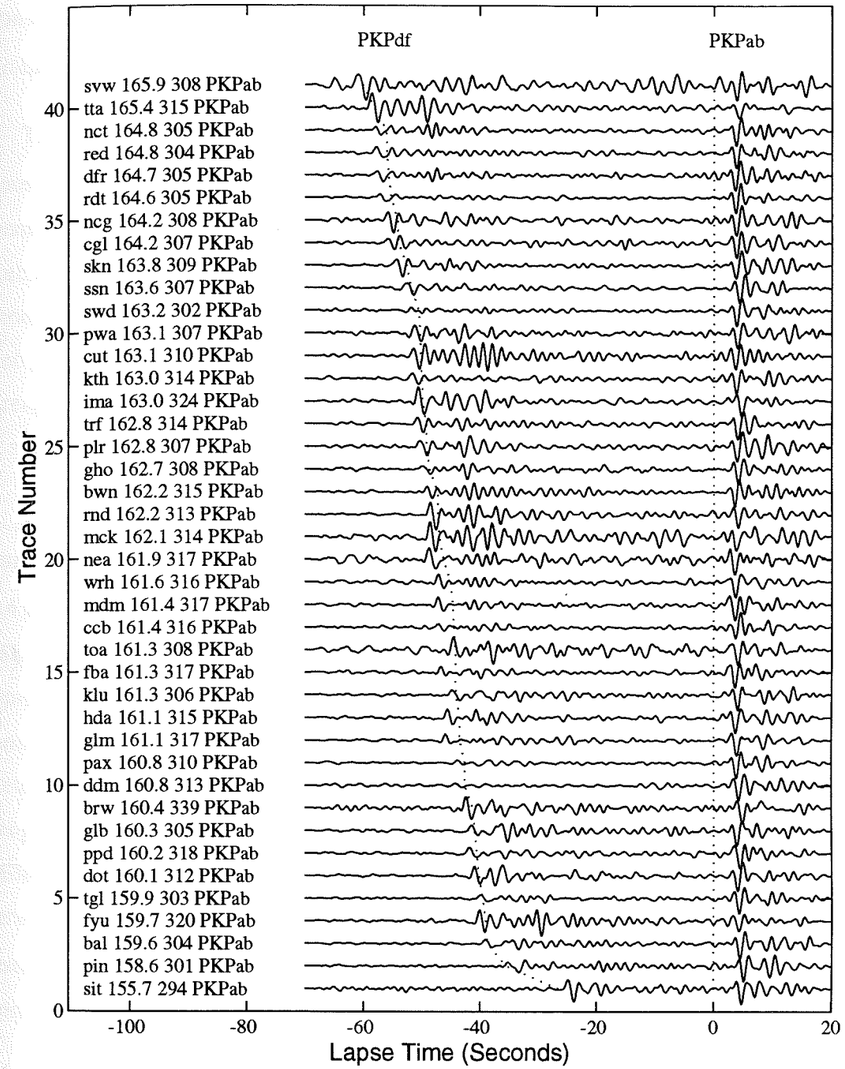

Figure 2-4: Vertical component seismograms from the Alaska Seismic Network aligned on the theoretical time for P'_{AB} in the epicentral distance range 155.7° to 165.9°. Dashed lines display theoretical travel times of P'_{DF} and P'_{AB}. The observed differential travel times consistently exceed the theoretical differential times by 4–6s. Station WRH is shown in detail in Figure 2-2. Numbers to the right of station names are epicentral distance and azimuth. Time is in seconds after P'_{AB} arrival.

tion technique after correcting P'_{AB} for the Hilbert Transform (Figure 2-2c and d). Note the similarity in waveform shapes after applying the Hilbert Transform.

These large P'_{AB}–P'_{DF} residuals lie along the trend defined by the P'_{BC}–P'_{DF} observations from the same array, resulting in a rapid increase of residual size with increasing epicentral distance from 2.5s at 150° to 5.5s at 163° (Figure 2-3a). Ray length in the inner core increases by 50% from 1400km at 150° to 2000km at 163°, whereas the travel-time anomalies increase by more than a factor of two. At greater epicentral distances, the rays also turn deeper into the inner core. This observation leads to our conclusion that the strength of the anisotropy increases from just under 3% at a radius of 950km to about 4% at a radius of 700km.

There are only five observations with ξ less than 40° and distances exceeding 165° (turning depths less than 500 km). These times have a mean and standard deviation of 4.4 ± 0.6 s. These residuals are smaller than the 37 observations in the distance range 158–165°, suggesting that anisotropy decreases with depth below 500 km. However, they represent only five observations, and the 1s decrease in residuals from the 158–165° distance range is of the order expected from the CMB. Thus, more observations should be collected at distances beyond 165° before a firm conclusion can be made. The improved geographic distribution of the IRIS/GSN and Geoscope seismic arrays may provide observations to extend the sampling to greater depths. For example, Vinnik et al. [1994] observed P'_{AB}–P'_{DF} differential travel-time anomalies of 3 to 6s at distances of 170–175° to station SEY which lies 2500km west of Alaska, from five earthquakes in the South Sandwich Islands.

CALNET: We picked 135 P'_{BC}–P'_{DF} times and 105 P'_{AB}–P'_{DF} times from the CALNET regional array in northern California for event 5 (Table 2-1, page 25). Both sets of residuals, displayed as open and closed circles in Figure 2-3, exhibit systematic trends as a function of epicentral distance, and very little scatter around these trends. The P'_{AB}–P'_{DF} residuals are consistently about 1s more negative than the P'_{BC}–P'_{DF} residuals, suggesting

that much of the anomaly is caused by deep-mantle structure where the P'_{AB} and P'_{DF} phases are well separated.

The positive slope of the P'_{BC}–P'_{DF} times versus distance from 152–155° (Figure 2-3a) is consistent with the slope in the GDSN observations, although the CALNET observations are offset down by about half a second. This slope is consistent with the model PREM2 of Song and Helmberger [1993b] which has lower velocities at the base of the outer core than PREM.

The ray angle, with respect to the spin axis, for the CALNET observations is 42–45°, a direction along which most anisotropy models predict moderately positive P'_{BC}–P'_{DF} times. However, our observed CALNET residuals are consistently negative. The observed P'_{BC}–P'_{DF} times are consistently 1.0 to 1.5s more negative than the predictions of Creager's [1992] model. These observations diverge from the simple anisotropy models more than any other P'_{BC}–P'_{DF} observations we are aware of. They may be indicative of heterogeneity in the inner core, or at the base of the outer core. Even though these represent many observations, the station spacing is very close and this represents the sampling of one small region of the Earth, but there is something very interesting going on along this path.

The discrepancy between the observed P'_{AB}–P'_{DF} residuals and those predicted by anisotropy models is even greater than that of the P'_{BC}–P'_{DF} residuals, but this could easily be explained by anomalously fast structure in D" along the P'_{AB} branch. Indeed, P'_{AB} exits the CMB under a point just south on Mexico, which is among the fastest D" regions in recent maps of Li and Romanowicz [1994].

2.3 Interpretation

Prior to inverting these data for a model of structure in the inner core, we discuss their geographic and directional sampling of the Earth in order to isolate the part of the Earth that gives rise to these times. The results are summarized in Figures 2-3 and 2-5 to 2-8.

Inner-core heterogeneity or Anisotropy? Figure 2-5 displays the observed differential travel-time residuals as a function of the angle (ξ) between the P'_{DF} ray at its turning point and the Earth's spin axis. The data are divided into four groups based on the turning radius (r_t) of the P'_{DF} phase: (a) r_t=900–1220 km, Δ=147–154°; (b) r_t=700–900 km, Δ=154–161°; (c) r_t=500–700 km, Δ=161–167°; and (d) r_t=0–500 km, Δ=167–180°. Large positive residuals are consistently observed at ray angles less than about 40°, suggesting an explanation in terms of anisotropy in the inner core with the fast axis parallel to the spin axis. At ray turning radii less than about 900km (Figure 2-5, b–d), times corresponding to ray angles near 60° are somewhat slower than equatorial directions ($\xi \sim 90°$).

Because P'_{DF} rays are nearly straight lines in the inner core, their directions can be specified by two angles. Consider a ray segment through the inner core. Translate the ray, without changing its direction, so it intersects the Earth's center. We can then describe the ray direction by the colatitude and longitude where the translated ray crosses the inner-core boundary in the southern hemisphere. These directions and the corresponding residuals are displayed in a lower hemisphere equal area projection (Figure 2-6). Points in the center of the plot represent rays parallel to the spin axis, while those near the edges are nearly perpendicular to the spin axis. As was clear in Figure 2-5, times corresponding to small ray angles display large positive residuals. However, this figure also shows that ray directions in the inner core are not uniformly sampled by the waveform data we have analyzed to date. In particular, nearly all of the rays with colatitudes less than 30° and turning point radii less than 700km are in the longitude range -20° to 50°. These correspond to earthquakes from the Sandwich Islands, and spreading centers in the South Atlantic and Indian Oceans to stations in Alaska and northern Canada. Shearer [1994] displays P'_{DF} travel-time residuals from the ISC data in the same projection. The values and distribution of ISC times at angles close to the spin axis are each about the same as for our waveform data. The ISC exhibits better coverage for paths that are not parallel to the spin axis, but are subject to possible picking problems. Also, these are absolute P'_{DF} times and may be contaminated by aspherical structure throughout the Earth.

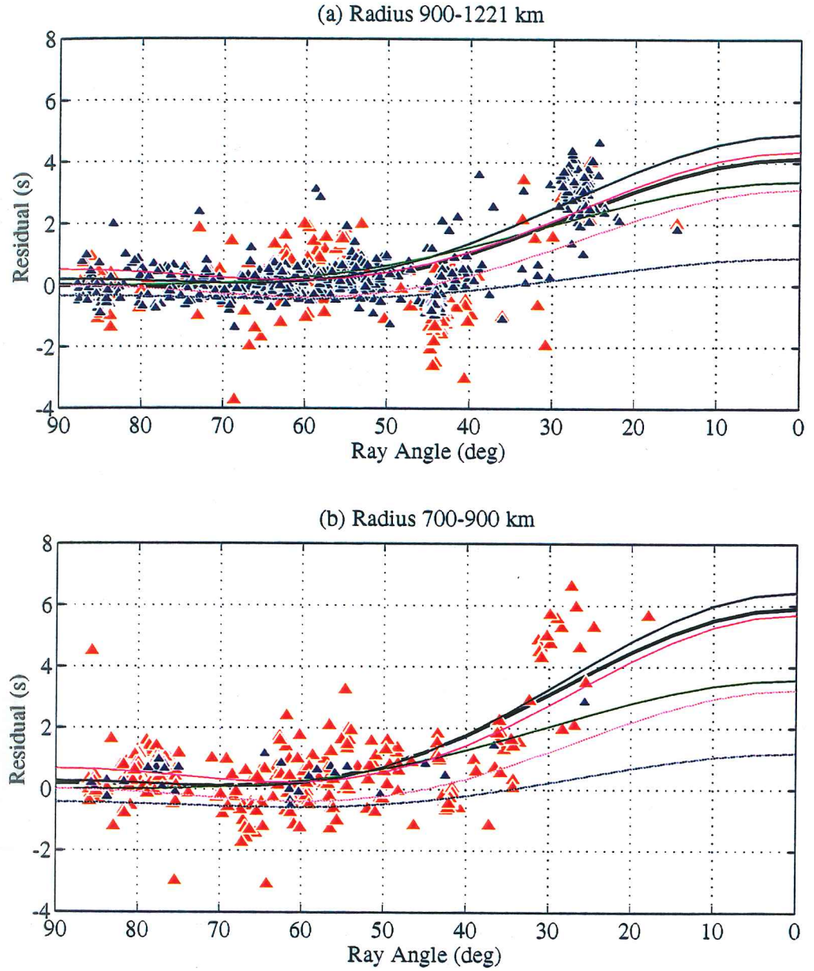

Figure 2-5: Differential travel-time residuals (P'_{BC}–P'_{DF} (blue) or P'_{AB}–P'_{DF} (red)) with respect to PREM versus ray direction (ξ) with respect to the spin axis, grouped by P'_{DF} turning point radius (r_t). (a) r_t = 900–1220 km, Δ=147–154°; (b): r_t = 700–900 km, Δ=154–161°; (c): r_t = 500–700 km, Δ=161–167°; and (d): r_t = 0–500 km, Δ=167–180°. Predicted times are also shown evaluated for rays turning at radii of 1000, 800, 600, and 400km for several models of inner-core seismic anisotropy. Included are predicted times for: our AXSYM model (thick black), Creager (1992) (thin black), Tromp (1993) (green), Morelli et al., (1986) (purple), Shearer et al., (1988) (dark blue), and Song and Helmberger, (1993) (magenta).

(c) Radius 500-700 km

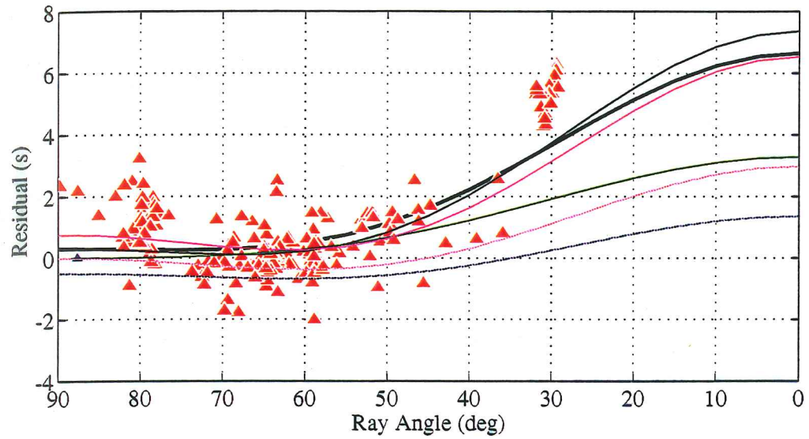

(d) Radius 0-500 km

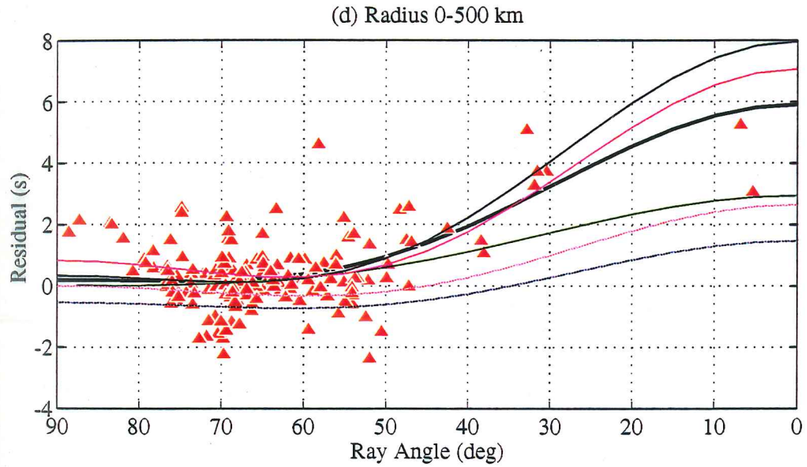

Figure 2-5 (continued): Differential travel-time residuals (P'_{BC}–P'_{DF} (blue) or P'_{AB}–P'_{DF} (red)) with respect to PREM versus ray direction (ξ) with respect to the spin axis, grouped by P'_{DF} turning point radius (r_t). (a) r_t = 900–1220 km, Δ=147–154°; (b): r_t = 700–900 km, Δ=154–161°; (c): r_t = 500–700 km, Δ=161–167°; and (d): r_t = 0–500 km, Δ=167–180°. Predicted times are also shown evaluated for rays turning at radii of 1000, 800, 600, and 400km for several models of inner-core seismic anisotropy. Included are predicted times for: our AXSYM model (thick black), Creager (1992) (thin black), Tromp (1993) (green), Morelli et al., (1986) (purple), Shearer et al., (1988) (dark blue), and Song and Helmberger, (1993) (magenta).

(a) Radius 900-1221 km

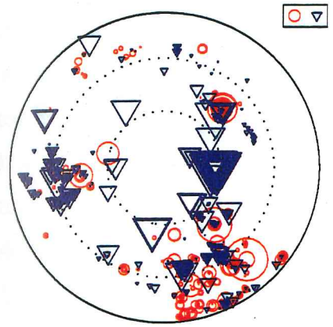

(b) Radius 700-900 km

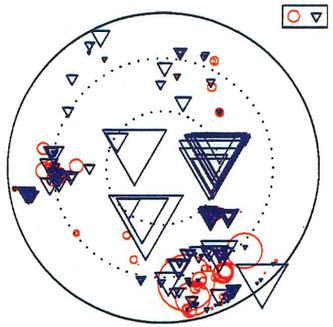

(c) Radius 500-700 km

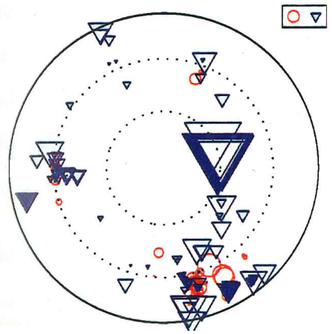

(d) Radius 0-500 km

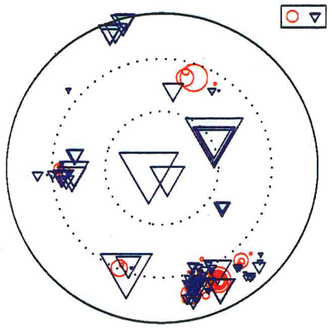

Figure 2-6: Differential travel-time residuals (P'_{BC}–P'_{DF} or P'_{AB}–P'_{DF}) as a function of inner-core ray direction displayed on an equal-area, azimuthal projection of the Southern Hemisphere. Ray direction latitude is 90°S at the center and 0° at the circumference. The longitude of the ray direction in the Southern Hemisphere is measured counterclockwise from the right of the diagram as if you were looking at the Earth down from the North Pole. Times are grouped by ray turning point radius as in Figure 2-5. Circles represent negative residuals, triangles are positive. One second residuals are shown in the box for scale.

The question of whether the 2–6s positive residuals are caused primarily by anisotropy in the inner core or isotropic heterogeneity in the core or mantle is assessed by displaying the data relative to geographic and directional sampling of the rays. Figure 2-7 shows the residuals and ray directions plotted at the ray turning points. Solid blue bars represent the large positive residuals, the ray angle (ξ) can be measured from north on these diagrams with a protractor. Rays within 40° of the spin axis sample the inner core just north of the equator from 270°E (Figure 2-7a) nearly continuously to 30°E (Figure 2-7d). These rays, which sample a full 120° of longitude all show large positive residuals. Many other rays in our study sample within 40° of the spin axis and are uniformly distributed over the remaining 240° of longitude. Six have large positive residuals, and are located at longitudes of 75, 100, 125, 130, and 235 (Figure 2-7a), and near Hawaii (Figure 2-7b). The only one with a negative residual is an P'_{AB}–P'_{DF} residual near India (Figure 2-7a). There are numerous observations corresponding to rays turning beneath northern South America, northern Africa and eastern Europe which sample similar geographic parts of the inner core to the times discussed above, but at ray angles exceeding 40° which generally have small residuals. This dependence on ray angle and not geographic location argues strongly in favor of an explanation in terms of anisotropy.

Because the P'_{BC} and P'_{DF} phases follow very similar ray paths throughout the Earth except near the turning point where P'_{DF} enters the inner core and P'_{BC} turns near the base of the outer core (Figure 2-1), this phase pair is ideally suited for imaging the inner core. In the mantle, including D", these rays remain within 300km of one another. We observed consistent 3 second P'_{BC}–P'_{DF} residuals to station COL from an array of 20 sources with an aperture of 500 km, as well as 97 times from 3 earthquakes to a 1000km aperture receiver array (ASN). This geometry of large-aperture source and receiver arrays, combined with small divergence of the P'_{BC} and P'_{DF} rays for each observation cannot be plausibly explained by structure in the mantle or in the vicinity of the CMB.

CMB heterogeneity? Unfortunately, the P'_{BC} phase can only be used as a reference

(a) 900-1221 km

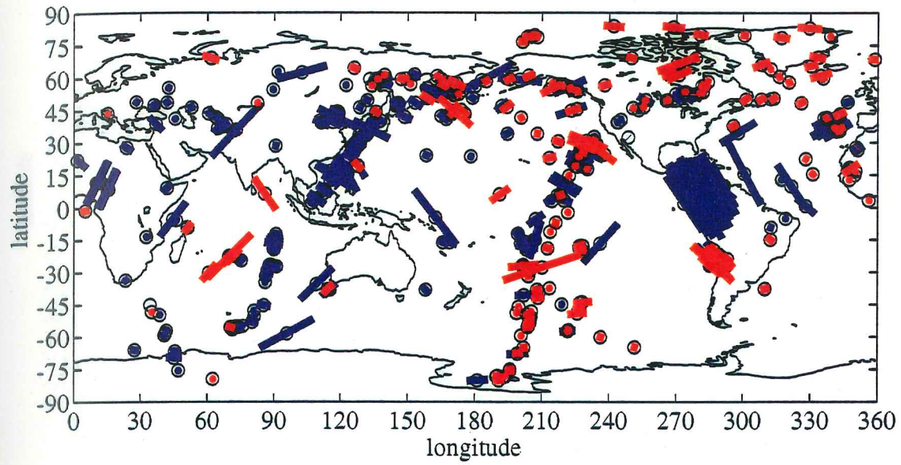

(b) 700-900 km

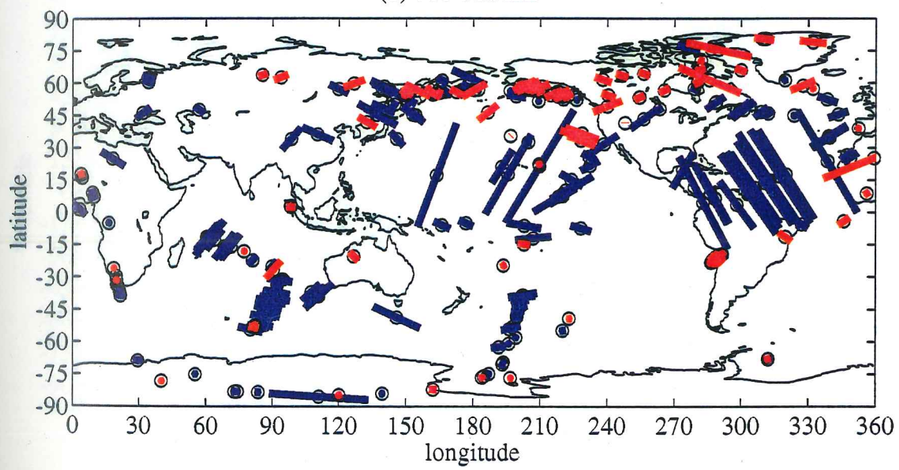

Figure 2-7: Differential travel-time residuals displayed at ray turning points. Blue represents positive residuals, red is negative. Residuals are proportional to line lengths. The angle between the lines and the latitude axis equal the ray angle in the inner core (ξ). Times are grouped by ray turning point radius as in Figure 2-5.

(c) 500-700 km

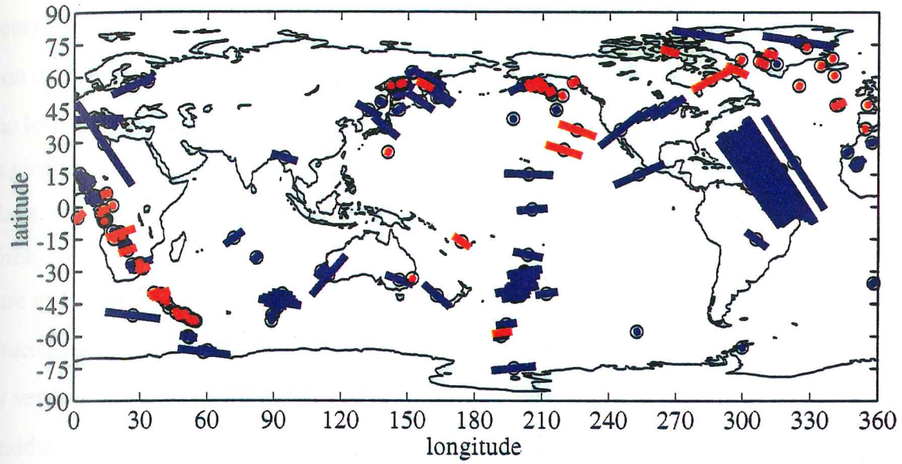

(d) 0-500 km

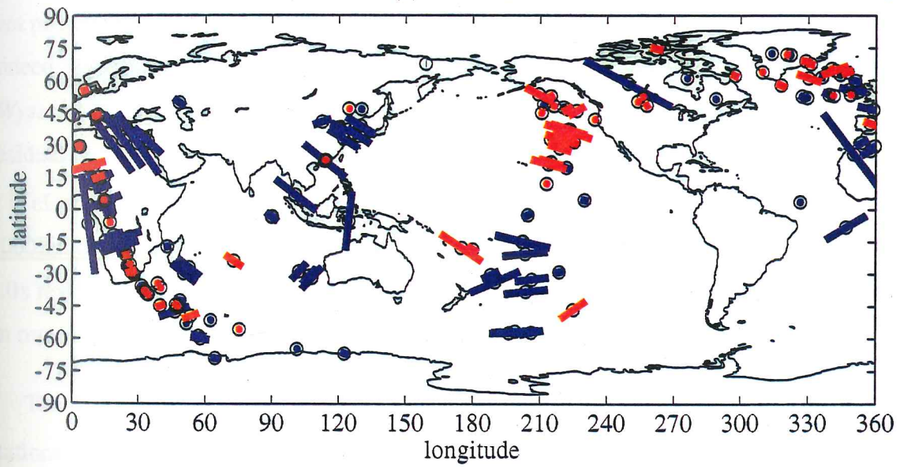

Figure 2-7 (continued): Differential travel-time residuals displayed at ray turning points. Blue represents positive residuals, red is negative. Residuals are proportional to line lengths. The angle between the lines and the latitude axis equal the ray angle in the inner core (ξ). Times are grouped by ray turning point radius as in Figure 2-5.

phase out to about 154° where it begins to diffract around the inner core. The P'_{DF} branch at this distance turns at a radius of about 900km (or a depth of about 300km into the inner core). To look deeper into the Earth we analyze the phase pair P'_{AB}–P'_{DF}. The interpretation of this phase pair is more ambiguous than P'_{BC}–P'_{DF} because the ray paths diverge in the lower mantle, especially near the CMB (Figure 2-1). Also, the take-off angle difference is greater, so this phase pair is more sensitive to near-source structure, say from descending slabs, and may also be sensitive to the effects of earthquake mislocation [*Helffrich and Sacks*, 1994]. In fact, this differential travel-time pair is well suited for imaging the structure of D" because the P'_{AB} branch approaches the CMB at a grazing angle and can be as much as six times more sensitive to D" structure as the P'_{DF} ray which approaches D" nearly vertically (Figure 2-1). One way to assess the contribution of D" structure to P'_{AB}–P'_{DF} residuals is to plot the residuals at the CMB entry and exit points of the P'_{AB} ray (Figure 2-8a). There are regions such as southeastern Australia to east of Hawaii which show consistent positive residuals, that may be caused primarily by aspherical structure near the CMB. Indeed, these residuals are qualitatively consistent with shear-wave velocity maps of D" [*Wysession et al.*, 1994]. However, with the exception of the pole-parallel paths, the rms residual of the P'_{AB}–P'_{DF} picks from the globally distributed GDSN is 1.0s. Furthermore, it is clear from this figure that these residuals show spatial coherence on length scales of 1000km or more, suggesting that random reading errors are generally small. The observed 1.0s residuals scale to lateral variations in compressional wave velocities within D", with an rms level of 1.5%, assuming D" is 200km thick.

The 4 to 6.5s P'_{AB}–P'_{DF} residuals consistently observed at the ASN and GDSN/GSN stations lie four to six standard deviations from the mean of the globally distributed GDSN/GSN times. It would take an unusual structure in the mantle to explain these observations. Furthermore, there are observations sampling the same regions of the CMB of significantly smaller (or even negative) P'_{AB}–P'_{DF} differential travel times for rays traveling in an East-West direction. For example, ray paths from events in Indonesia to stations in South Amer-

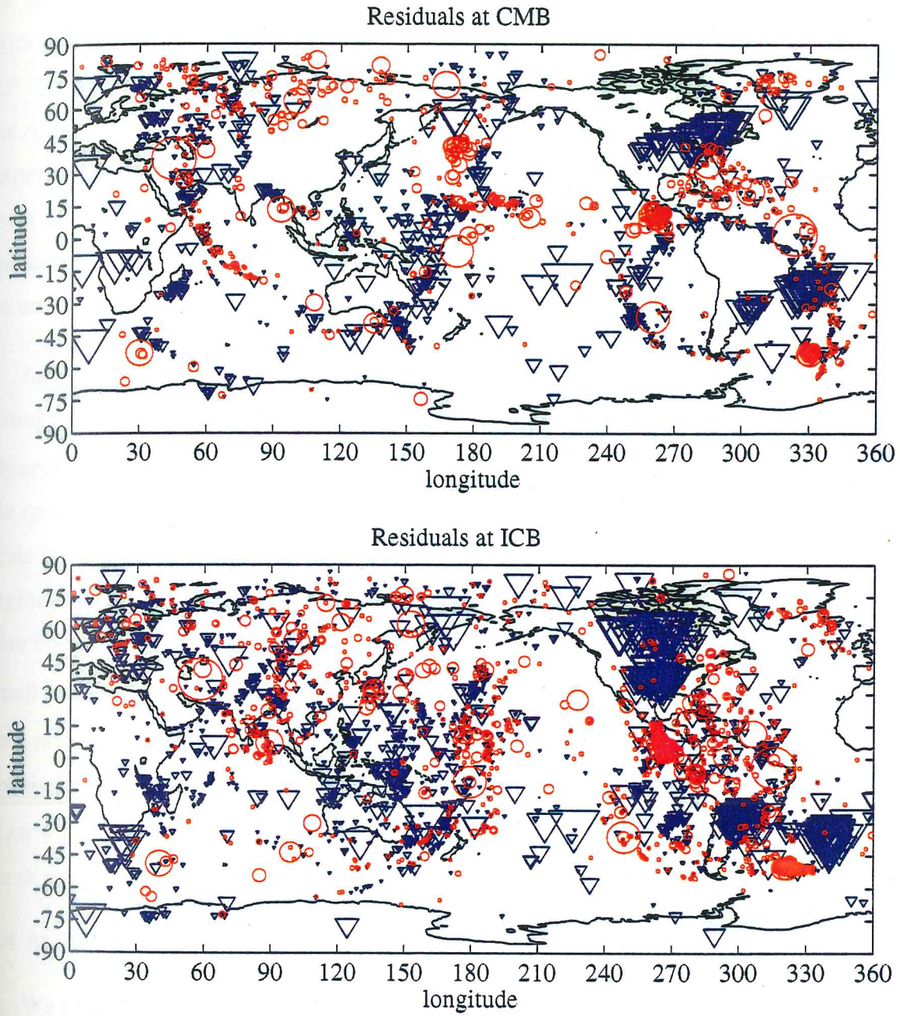

Figure 2-8: Differential travel-time residuals plotted (a) at CMB interaction points of their P'_{AB} rays and (b) at the inner-core boundary interaction points of the P'_{DF} rays. Triangles represent positive residuals (fast inner-core velocity or slow CMB velocity at the P'_{AB} point), circles are negative. Residuals (s) equal symbol height (deg) divided by 4.

ica enter the CMB under the Indian Ocean and exit the CMB under the South Atlantic, at the same location that rays going to the ASN enter the CMB. This set of crossing paths is difficult to explain using isotropic CMB structure, because there would have to be a nearly 70° "patch" at the CMB that is slow with respect to PREM to explain the array data from the ASN. If this were the case, the small residuals observed for the Indonesian events would require a huge velocity anomaly under the Indian Ocean of opposite sign. A similar argument can be made for the exit points of the ASN observations (North America) which are coincident with east-west paths whose residuals are small and whose other sample points lie under Russia.

Inner-core Heterogeneity? The level of isotropic heterogeneity in the inner core is most strongly limited by the globally distributed, and small differential travel times (P'_{BC}–P'_{DF}) observed by Shearer and Toy [1991] and Creager [1992]. For paths not near the spin axis the rms variation is only 0.4s. Travel times through the inner core exceed 100 s, so large-scale inner-core heterogeneity in the inner core is typically less than 0.5%, at least in the regions that were sampled. Figure 2-8b shows the differential times displayed at the inner-core boundary interaction points of the P'_{DF} rays. The P'_{BC}–P'_{DF} times are invariably very small (except for the pole-parallel paths). For example, P'_{BC}–P'_{DF} times in the North Pacific invariably correspond to the very small symbols whereas the large, yet geographically consistent, residuals such as the circles south and east north east of Japan all correspond to P'_{AB}–P'_{DF}. This suggests that heterogeneity in the outer 300km of the inner core is very weak relative to that in D".

2.4 Modeling

We model the differential travel-time residuals using a perturbation to PREM in the inner core of the form:

$$\delta v(r,\xi) = f_0(r) + f_1(r)\cos^2\xi + f_2(r)\cos^4\xi \qquad 2\text{-}1$$

where r is radius and ξ is the ray angle the P'_{DF} ray makes in the inner core with respect to an assumed symmetry axis of the anisotropy. This axis need not be the spin axis of the Earth. Compressional velocity perturbations for weak anisotropy with a cylindrical symmetry can be approximated with this form. This is the same form used by Creager [1992] except that in his study the functions $f_i(r)$ were taken to be constants. This form is equivalent to, though notationally different from, the models proposed by Morelli et al. [1986], Shearer et al. [1988], Shearer and Toy [1991], Song and Helmberger [1993a], and Tromp [1993]. Analytic conversion factors are given by Creager [1992] and Tromp [1993].

For the PREM velocity model, the segment of theoretical ray paths which lie in the inner core are perfect circles. Within the inner core, no P'_{DF} ray bends by more than $\pm 1.3°$ from its direction at the turning point. For the purposes of modeling, we assign the ray angle ξ appropriate to the ray turning point, and assume it is constant along the ray. Following Tromp [1993], we used cubic B-splines as our basis functions (denoted here by $g_m(r)$ for m = 0–4) with five equally spaced knots in the inner core. The formula for these basis functions are given by Michelini and McEvilly [1991]. They are plotted by Tromp [1993]. Using these basis functions, the $f_n(r)$ values given in equation 2-1, above, can be rewritten as:

$$f_n(r) = \sum_{m=0}^{4} b_m^n g_m(r) \qquad \{n = 1, 2, 3\} \qquad 2\text{-}2$$

The observed travel-time anomalies are given to first order in δv by:

$$\delta t = - \int_{raypath} \frac{\delta v(\xi, r)}{v(r)^2} ds \qquad 2\text{-}3$$

where $v(r)$ is the compressional wave speed for PREM, and the integral is over ray paths through the inner core. Putting (2-1) and (2-2) into (2-3) leads to a linear system of equations relating the observed differential travel-time anomalies δt to the 15 spline coefficients b_m^n, which describe the model. These equations can be put in the standard form:

$$\delta t = \boldsymbol{A} \cdot \boldsymbol{b} \qquad 2\text{-}4$$

where $\delta\mathbf{t}$ contains the 1730 differential travel-time observations, **b** is a vector containing the 15 spline coefficients, and **A** is a matrix whose elements are determined using the integral (2-3), along ray paths.

Prior to inversion, we weight the data using an estimate of their uncertainties of the form:

$$\sigma_i^2 = \sigma_P^2 + N_i \, \sigma_S^2 \qquad 2\text{-}5$$

where the uncorrelated picking uncertainty is given by $\sigma_P = 0.3$s and potentially correlated errors owing to unmodeled earth structure are given by $\sigma_S = 0.5$s for P'_{BC}–P'_{DF} and σ_S = 1.0s for P'_{AB}–P'_{DF}. These are the values of the standard deviations of our GSDN observations at ray angles exceeding 40° from the spin axis. N_i is the number of rays whose inner-core boundary entry and exit points each lie within one degree of those for the i^{th} ray. This down weights redundant data which could have correlated errors owing to the fact that they each sampled the same structure outside the inner core. N_i equals one for most of the GDSN observations, but can be as large as 30 for the CALNET observations.

Each row of (2-4) is divided by σ_i and the model coefficients are determined using:

$$\boldsymbol{b} = \left[\boldsymbol{A}^T\boldsymbol{A} + \gamma \boldsymbol{I}\right]^{-1}\boldsymbol{A}^T\delta\boldsymbol{t} \qquad 2\text{-}6$$

Where the regularization parameter γ has been chosen by analyzing the trade-off curve [*Parker*, 1994]. For all models in this study, we chose γ such that 7 of the possible 15 degrees of freedom of the model space were kept. In order to avoid extrapolations of the model to large velocity perturbations at small values of ξ and r, we have severely damped the inversion. As a result the very large P'_{AB}–P'_{DF} residuals observed at large epicentral distances to the ASN are systematically under estimated by about 1.5s (times at ξ=30° in Figure 2-5b and c, and the blue diamonds in Figure 2-3b).

Whereas the relation between the observations and the spline coefficients is linear, the travel times are a highly nonlinear function of the symmetry axis direction assumed for the cylindrical anisotropy. We search for the best symmetry axis by performing a linear inver-

sion of the data for a radially varying model of anisotropy at each of 1297 fixed symmetry axis positions, spaced equally at 5° increments in colatitude and longitude. Figure 2-9 shows the resulting weighted variance reductions plotted at symmetry-axis positions projected onto a southern-hemisphere equal-area projection. Our best fitting model has a symmetry axis located at 80°S, 350°E, only 8.5° from the best model obtained by Creager [1992]. The variance reduction of the best fit model (called AXOFF) is 59%, 3% better than that for the axisymmetric model (AXSYM). The spline coefficients for each of these two models are given in Tables 2-2 and 2-3 and the velocity perturbations are displayed as a

Table 2-2: Spline Coefficients for Axisymmetric Model

n	b_0	b_1	b_2
0	0.0322	0.0018	–0.0008
1	–0.0253	–0.0304	0.0005
2	0.0310	0.0478	0.2200
3	0.0101	–0.0977	0.3763
4	-0.0072	–0.1004	0.3117

Table 2-3: Spline Coefficients for Best Fit (Axis Offset) Model

n	b_0	b_1	b_2
0	0.0249	0.0023	-0.0002
1	–0.0137	–0.0281	0.0041
2	0.0255	0.0323	0.2122
3	0.0223	–0.1442	0.3531
4	0.0025	–0.1556	0.3021

function of radius and ray angle in Figure 2-10. The two models are very similar. They show an increase in the amplitude with decreasing radius from 1200 to 700km, followed

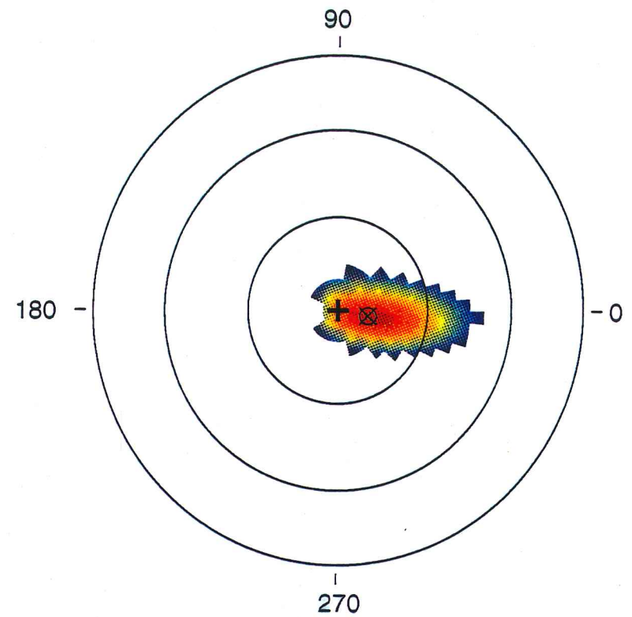

Figure 2-9: Percent variance reduction plotted against the symmetry direction of models of depth-varying anisotropy with cylindrical symmetry. The projection is described in Figure 2-6. The "best" fit model has a symmetry axis at 80°S, 350°E (circle and cross). The variance reduction for this model is only 3% better than that for the axisymmetric model.

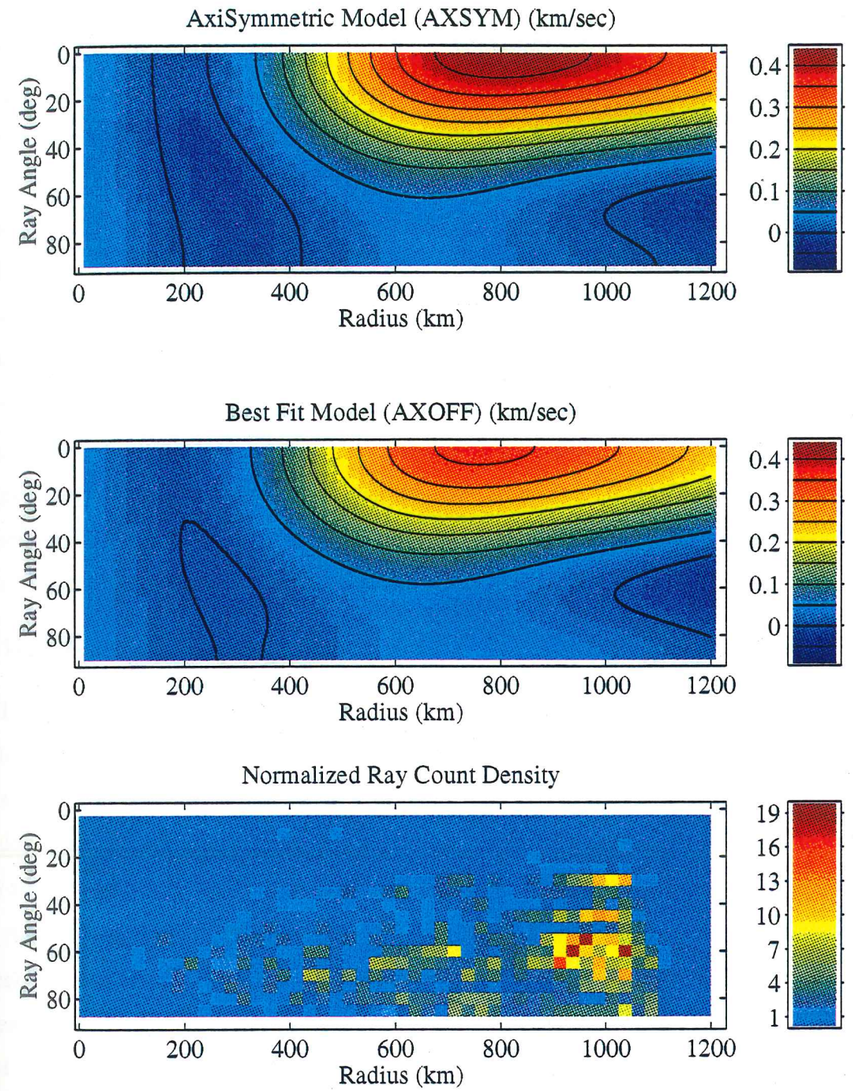

Figure 2-10: Surface plots of velocity perturbations (km/s) to PREM for the axisymmetric model AXSYM (a), the axis offset model AXOFF (b), and normalized ray-count density (c), each as functions of ray turning radius and ray angle (ξ). Note that there is little sampling at radii below about 400 km, and at ray angles less than 25° so these regions of our models are poorly constrained. Ray counts are normalized by N_i as described in eqn. 5, and show the number of normalized rays per 5° bin in ξ and 25km bin in radius.

by a decrease in anisotropy. The anisotropy in AXSYM, characterized by the velocity parallel to the spin axis versus that normal to this direction varies from under 3% in the outer 200 km, raising to a peak value of 4% at 700km radius and falling to near zero below 300km. However, our model is poorly constrained at great depths because there are very few observations at both large distances and small ξ values. As a result, some of the decrease in anisotropy at great depths may be the result of the regularization applied during the inversion process. Our model is also poorly constrained at shallow depths, near the inner-core boundary, since all event-station pairs with distances less than 147° were not used in this study (the waveforms for the P'_{BC}, P'_{AB} and P'_{DF} phases overlap, preventing the determination of accurate differential travel times using a cross-correlation technique like ours), so the values of anisotropy at these shallow depths should also be used cautiously. Better estimates of the changes in anisotropy near the ICB are available in the results of studies by Song and Helmberger [1992] and Shearer [1994], both of which propose that the level of anisotropy decreases with increasing radius as the ICB is approached.

2.5 Discussion

There is a growing consensus that the inner core is strongly anisotropic with a fast direction parallel, or within about 10° of the Earth's spin axis. Figure 2-5 displays the predictions of many of the published models. Shearer et al.'s [1988] model was derived using windows that did not allow residuals greater than 1.5 s, and not surprisingly predicts only very small travel-time residuals (Figure 2-5). Shearer [1994] reanalyzed the ISC P'_{DF} times and finds that rays nearly parallel to the spin axis do indeed consistently exhibit large residuals, up to 5s for some paths. He did not invert for a specific model, but the ISC data appear generally consistent with our hand picked times. Song and Helmberger [1993a] hand picked times which sample regions that are geographically distinct from those presented here. Their data are consistent with AXSYM, and their model is similar (Figure 2-5). Vinnik et al. [1994] have measured P'_{AB}–P'_{DF} times for near pole-parallel paths (ξ=30°) to large epicentral distances (170–175°) and find 3–6s residuals. These lie systematically above the predictions of AXSYM (lower solid line in Figure 2-3a), but near the predictions

of Creager's [1992] model. To fit these observations, the anisotropy would have to decrease towards the center of the Earth below its peak value near 700km radius, but a less rapidly than in AXSYM. In this study, we have a few observations with similar distances and ray angles, but our data do suggest that there is a more rapid decrease in anisotropy with depth than their data suggest. This may be indicative of heterogeneity in the anisotropy of the inner core, but with the data available at the present time we cannot resolve this question. As will be discussed in Chapter 3, we feel that the differences between their observations and ours are most likely due to the effects of CMB structure on the P'_{AB}–P'_{DF} times used at these large distances. Finally, Tromp's [1993] model, constructed from normal modes, is consistent with rays turning in the outer 300km of the inner core, but it under predicts the residuals of our deeper penetrating rays. Given the non-uniqueness of the mode models, and the fact that resolution decreases with increasing depth, we anticipate that models similar to AXSYM will be consistent with the splitting observations.

Observations of P'_{DF} residuals at epicentral distances less than 145° turn in the upper 150km of the inner core, and can provide resolution of this region that is not attainable in our study. Shearer [1994] shows that models with 3% anisotropy in the outermost inner core systematically overpredict the observed ISC P'_{DF} times of pole-parallel paths by about 1s, suggesting that the anisotropy near the surface of the inner core is less than 3%. However, 1s anomalies can be easily caused by structure elsewhere in the Earth. The anisotropy in the outermost inner core can be robustly determined by measuring the P'_{CD}–P'_{DF} times at epicentral distances of 130–140° for pole-parallel paths using methods described by Cormier and Choy [1986], Cummins and Johnson [1988] and Song and Helmberger [1992, 1994 #123].

The symmetry axis that best fits our data is at 80°N, 170°E. This lies within 8.5° of the previously reported best fitting axis obtained by Creager of 80°N, 120°E [*Creager*, 1992] and within 2° of the best fitting axis obtained by Su and Dziewonski of $79.5 \pm 1°$ N, $160 \pm 5°$ E [*Su and Dziewonski*, 1994]. However, the model with respect to this "best fit"

symmetry axis fits the data only 3% better than the model who's symmetry axis coincides with the Earth's spin axis. The set of models which provide reasonable fits to the data, say variance reductions of 50–59% include the spin axis, but less than 4% of the range of possible symmetry directions. Thus, it is highly unlikely that the anisotropy symmetry axis is very close to the Earth's spin axis by random chance. We do not have sufficiently uniform sampling to determine with certainty whether the spin axis and the anisotropy symmetry axis coincide exactly.

The magnitude of anisotropy reported here is very large. Recent first-principle, quantum mechanical based calculations of predicted anisotropy at high pressure in hexagonal close packed (hcp) iron predict elastic anisotropy at about the 3% level, with the c-axis being fast [*Stixrude and Cohen*, 1995]. To produce the travel times we observe would require 100% alignment of iron crystals, an unlikely possibility. This apparent discrepancy between theory and observation requires further attention.

2.6 Brief Review of Dynamo Theory

Table 2-4 lists several possible mechanisms that could give rise to large-scale seismic anisotropy in the inner core. We will divide these mechanisms into two groups: class I, which has no important implications for Geodynamo Theory, and class II, which does.

Table 2-4: Possible Models that Produce Inner-Core Seismic Anisotropy

Model #	Description	Class	Reference
1	Solid-State Convection	I	Jeanloz and Wenk (1988)
2	Paramagnetic Mechanism	II	Karato (1993)
3	Crystal Growth in Magnetic Field	II	this paper
4	Settling Mechanism	I	this paper
5	Rotational Shear in "Mush Zone"	probably II	this paper

Before discussing these mechanisms in detail, it is useful to provide some background in dynamo theory. The reader who wants a more detailed discussion of modern dynamo theory is referred to Gubbins and Roberts [1987], Roberts and Gubbins [1987] and Roberts [1987].

Dynamo Theory often starts with the magnetic induction equation:

$$\frac{\partial \boldsymbol{B}}{\partial t} = \kappa \nabla^2 \boldsymbol{B} + \nabla \times (\boldsymbol{v} \times \boldsymbol{B}) \qquad 2\text{-}7$$

where $\boldsymbol{B}$ is the magnetic induction, t is time, κ the magnetic diffusivity, and $\boldsymbol{v}$ the velocity field. Equation 2-7 illustrates that the magnetic field (linearly related to $\boldsymbol{B}$) changes in time via diffusion (the first term on the right side of 2-7) and fluid advection (the second term on the right side of 2-7). The solution to the geodynamo problem not only involves solving equation 2-7, but also simultaneously solving other partial differential equations such as those for heat flow and fluid motion. These equations are often coupled to each other and involve non-linearities. In addition, many of the physical parameters that are involved in the equations are not well known. A consequence of this is that there is no adequate dynamo model for the Earth. Instead, there are numerous models that are inadequate in one way or another [*Merrill and McFadden*, 1995]. To simplify the discussion here, the terminology subsequently used in this paper refers primarily to mean-field dynamo models.

The magnetic field in the core is commonly divided into the toroidal magnetic field, which is divergence free and has no radial component, and the poloidal magnetic field, which is curl free and has a radial component [*Merrill and McFadden*, 1983]. The strength of the poloidal magnetic field in the core can be obtained by various methods of downward continuation, while the strength of the toroidal magnetic field in the core must be inferred from theory because the toroidal magnetic field rapidly decays in the mantle. Dynamo models that posit a strong global toroidal magnetic field usually assume this field has rotational symmetry.

Figure 2-11 illustrates how such a toroidal field can originate when there is rotational shear and in the frozen-in-flux approximation (negligible diffusion, i.e. κ in equation 2-7

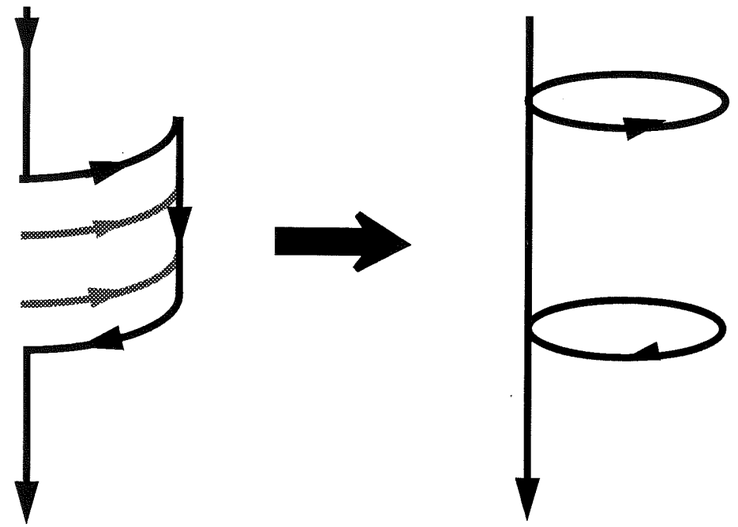

Figure 2-11: Generation of a toroidal magnetic field from a poloidal field by large scale (toroidal) rotational shear (an ω-effect). For the purpose of illustration, we assume frozen-in-flux (κ=0 in eqn 7). The solid line represents a magnetic field line, while the grey lines show fluid velocity. There is no fluid flow at the top and bottom. There is rotational flow near the center. Strong shear occurs along the two horizontal planes separating these regions. From a poloidal (vertical) field line, a new pair of opposing toroidal loops is constructed for every complete circle of fluid flow because the field lines are carried along by the fluid. This process is denoted as ωST.

can be set to zero). Theory and indirect observations indicate that the strong-field regime (defined in the next section) is appropriate to the Earth's core [*McFadden et al.*, 1985; *Roberts*, 1987]. However, there is no consensus that there must be a global scale toroidal field or even if a global toroidal field exists, that it must have rotational symmetry. The process by which a toroidal, T, magnetic field is produced from a poloidal, S, field by large scale rotational shear is often denoted symbolically by ωST (see Figure 2-11). This is the so-called ω-effect of geodynamo theory in which rotational shear converts fluid mechanical energy to magnetic field energy.

To produce a dynamo, the toroidal magnetic field must be acted on by the fluid to convert some of its energy back to a poloidal magnetic field. Often this is done by evoking an α-effect. In mean-field dynamo models it can be shown that an α-effect occurs when there is a correlation between perturbations in the velocity field, **v'**, and the resulting variable magnetic field, **B'**, i.e. the average value of **v'**×**B'** is not zero [*Merrill and McFadden*, 1995]. The process of taking a toroidal magnetic field to a poloidal one by an α-effect is denoted by αTS. When the two processes, αTS and ωST, combine to produce a dynamo, the dynamo is referred to as an αω dynamo. It is also possible through the α-effect to take an initial poloidal magnetic field and produce a toroidal magnetic field: this process is denoted by αST. The combination of the two processes, αST and αTS, can lead to an α^2 dynamo. Moreover it is possible that an αST and an ωST process both occur to produce a toroidal magnetic field. When they are combined with an αTS process, this can lead to an $\alpha^2\omega$ dynamo.

In theory, large scale toroidal fields can also be produced by thermal-wind driven fluid motions associated with small temperature differences at the CMB. These temperature differences are substantially less than a degree; the CMB is essentially an isothermal boundary [*Gubbins and Roberts*, 1987].

Some of the mechanisms discussed below require the presence of a toroidal magnetic field in the inner core. If such a field exists in the inner core, it does so by diffusion of a

toroidal field from the outer core. Characteristic times for diffusion of the field can be obtained by taking $\mathbf{v} = 0$ in (2-7) and by assuming a solution of the form $\mathbf{B} = \mathbf{B}_0 \exp(-t/\tau)$. Then (2-7) reduces to

$$\nabla^2 \boldsymbol{B}_0 + \frac{1}{\kappa\tau}\boldsymbol{B}_0 = 0 \qquad 2\text{-}8$$

Equation 2-8 can be solved by using vector spherical harmonics along with appropriate boundary conditions [*Elsasser*, 1946; *Gubbins and Roberts*, 1987]. Characteristic decay times for a poloidal field of degree l are the same as for a toroidal field of degree l+1. The magnetic diffusivity is inversely related to electrical conductivity, and for an electrical conductivity value near $5\text{x}10^5\,\text{S}\,\text{m}^{-1}$ [*McFadden and Merrill*, 1995], one obtains a characteristic decay time for the diffusion of a toroidal field of degree two into the inner core of the order of 1000 years. The uncertainty on this value is less than on order of magnitude [*Poirier*, 1991; *Stacey*, 1992]. Therefore if there is a toroidal magnetic field deep in the outer core, it is safe to conclude there will also be one in the inner core (having diffused there).

Another important variable of interest in this paper involves the strength of the magnetic field in the Earth's core. Usually dynamo field theoreticians describe the strength of the magnetic field by comparing the Lorentz force to the Coriolis force. The fluid motions in the Earth's outer core must satisfy the Navier-Stokes equation with the Lorentz force ($\mathbf{J}\times\mathbf{B}$, where $\mathbf{J}$ is the electric current density) included as a body force. One indication of the strength of this body force is given by the dimensionless Elsasser Number, Λ, which is a measure of the relative strength of the Lorentz force and the Coriolis force:

$$\Lambda = \frac{B^2}{(\rho\mu_0\kappa\Omega)} \qquad 2\text{-}9$$

where Ω is the magnitude of the Earth's angular velocity, ρ is the density of the fluid outer core, and μ_0 is the free air magnetic permeability. If Λ is much less than one, the Lorentz force can be neglected in calculating the fluid motions and the dynamo is said to be in the

weak field regime, while if Λ is one or greater, the dynamo is said to be in the strong field regime. Λ is close to unity when B (= |**B**|) is approximately three times the present dipole field strength at the CMB.

2.7 Mechanisms for seismic anisotropy and implications for dynamo theory

We are now in a position to discuss mechanisms that could result in seismic anisotropy and to speculate on the possible consequences with regard to geomagnetism. Table 2-4 (page 46) lists several possible mechanisms that could give rise to large-scale elastic anisotropy in the inner core. One mechanism, suggested by Song and Helmberger [1993a] is layering. A stack of thin isotropic layers of differing wave speeds produces a medium that appears anisotropic with cylindrical symmetry. Rays perpendicular to the layers are slow relative to those traveling in the plane described by the layers. A stack of layers oriented normal to the spin axis would produce the correct symmetry, but would be slow along the spin axis, opposite the observations for the inner core. Furthermore, the layering would have to produce a cylindrical symmetry, not a spherical symmetry, which one might expect for layering in the inner core. Therefore, this mechanism seems unlikely.

The other mechanisms are related to aligning the crystals that make up the inner core, assuming that the iron crystal are themselves anisotropic. The first mechanism suggested to explain seismic anisotropy was by Jeanloz and Wenk [1988], who suggested that solid state creep (perhaps due to slow convection) could be used to align hexagonal closest packed iron crystals (also denoted as hcp or ε-iron crystals). This mechanism does not involve magnetic fields and appears to have no important testable consequences for geomagnetism and, as a result, is classified as a class I mechanism in this paper. The only other published mechanism that we are aware of is that due to Karato [1993]. This mechanism has important implications for geomagnetism and is therefore a class II mechanism. Karato suggests that a paramagnetic mechanism could be used to dynamically align iron crystals in the inner core. Although the temperatures of the inner core are well recognized to be too high for permanent magnetism to exist there, it is possible that iron (in either its hexagonal or cubic form) has a significant paramagnetic component at the pressures and temperatures

of the inner core, i.e., it is capable of exhibiting an induced magnetic moment (positive susceptibility). The minimum energy state for such paramagnetic iron crystals would occur when the crystal's maximum susceptibly axis coincides with the local magnetic field, allowing the magnetic field to dynamically align the crystals after they had formed. However, as pointed out by Karato, the magnetic susceptibility of iron at the high temperatures of the inner core would likely be very small, so for this model to be valid the magnetic field must be strong.

There appear to be other mechanisms that could produce inner-core seismic anisotropy. To discuss these mechanisms, it is useful to discuss the transition zone between in inner and outer core. As more than one chemical substance is likely to be involved in the composition of the Earth's core [*Jacobs*, 1992], there is almost certainly a region that we will refer to as a "mush zone", in which a significant volume of liquid and solid material coexist. The rheological boundary of the inner core probably differs from the seismically defined inner-core boundary (or ICB). The rheological boundary, where there is a sharp increase in viscosity, probably occurs when the melt fraction drops below about 50% [*McFadden and Merrill*, 1995]. This boundary probably resides above the seismic boundary, below which shear waves can be transmitted. Two new mechanisms for seismic anisotropy that involve alignment of crystals in the "mush zone" and subsequent solidification to form the outermost part of the inner core are listed in Table 2-4 (page 46) If the crystals forming in the mush zone are not equidimensional, then during settling a lineation or foliation could develop. This is referred to as the Settling Mechanism in Table 2-4. The last mechanism presented in Table 2-4 (the rotational shear mechanism) also requires crystals that are non-equidimensional, but alignment occurs due to large scale rotational shear in the "mush zone". It is important to distinguish this mechanism from the settling mechanism, because the rotational shear mechanism can produce large-scale rotational symmetry, while the settling mechanism, by itself, cannot. Settling of crystals in a quiet fluid environment would produce large scale anisotropy in which seismic waves traveling along an Earth radius would travel at different velocities than waves traveling perpendicular to a radius. On the other

hand, large scale rotational shear in the "mush zone" could produce a preferential crystal orientation which exhibits symmetry about the Earth's rotational axis. Presumably, if such large scale rotational shear is present in the "mush zone", it is also present in the outer core due to magnetic coupling between the motions in the "mush zone" and those in the outer core. As a result, such rotational shear in the "mush zone" should produce a large scale toroidal magnetic field with rotational symmetry. The size of this magnetic field, of course, would be model dependent. The final mechanism that we speculate on here involves the growth of the crystals (as they form at or near the ICB) in a strong magnetic field. Since the magnetic field energy must be included in the free-energy of the crystal (e.g. it can effect the spin-orbit electronic coupling), it is conceivable that certain crystallographic axes will grow more efficiently when they are aligned parallel to the field lines of a strong magnetic field, rather than off of the field lines. This is listed as the third mechanism in Table 2-4 (page 46). If this "Crystal Growth" mechanism is valid, then it would also require a strong toroidal field in the Earth's core in order to give rise to the nearly rotationally symmetric seismic anisotropy that is observed.

Karato [1993] argued that the mechanism that produces solid state creep would not occur at inner-core pressures and temperatures (i.e. convection in the inner core was unlikely) and that his paramagnetic model, which requires a strong toroidal magnetic field, is the correct mechanism by default. We approach the problem from a different direction from that taken by Karato. We resist the temptation to evaluate the individual merits of the proposed anisotropy mechanisms for two reasons: often a good evaluation of individual mechanisms requires knowledge of core properties that are very poorly known (e.g. the paramagnetic susceptibility of inner-core material) and there may be new hypotheses for the origin of the anisotropy (e.g. there are more than double the mechanisms given above than were considered by Karato). Instead, we argue that it is the symmetry imposed by the seismic anisotropy that provides the strongest constraint, regardless of many of the details of the mechanism that produces the anisotropy. Class I mechanisms given above appear incompatible with the type of inner-core anisotropy observed (or effective anisotropy produced by small scale

heterogeneity), because there is no particular reason that the symmetry in the anisotropy of such models should be so consistently strong and axisymmetric over such a wide range of depth values. In the inner-core convection model of Jeanloz and Wenk [1988], for example, one would expect substantial changes in the "level" of anisotropy with the turning point depth of the rays as one crosses the "limbs" of the convection cells. On the other hand, all class II mechanisms considered here seem to either (a) require a strong toroidal magnetic field with rotational symmetry or (b) produce a toroidal field of some strength (weak or strong) that is both global and axisymmetric. The importance of the last conclusion with regard to dynamo theory appears to be much greater than seems to have been appreciated.

The discussion thus far has concentrated on effects associated with the time-averaged toroidal magnetic field. However, it should be pointed out that a strong poloidal magnetic field directed along the rotation axis could also produce the observed anisotropy by the mechanisms discussed above that involve a magnetic field. A poloidal field of this sort could originate from a mean toroidal electric field ring current in the outer core. There is no evidence for such a current. Moreover, in strong field dynamos the toroidal magnetic field is dominant and this appears also to be the case in the inner core even for dynamos for which the poloidal and toroidal fields in the outer core are of comparable size [*Glatzmaier and Roberts*, 1993]. Hence, although conceivable, this mechanism appears highly improbable.

2.8 Conclusions

We have analyzed 1730 differential travel times of PKP and PKIKP phases and find that PKIKP rays traveling nearly parallel to the spin axis are consistently 2 to 6 s faster than normal, depending systematically on ray bottoming depth. We argued that these large residuals do not appear to reflect heterogeneity in the crust, the mantle, the core-mantle boundary, or the inner core. The effects of inner-core attenuation are also inadequate, as is the apparent anisotropy owing to layering in the inner core. Hence, it appears that anisotropy due to preferred crystal alignment in the inner core is required. The inner core exhibits nearly axi-symmetric cylindrical compressional-wave anisotropy with the fast direction

parallel to the spin axis. The level of anisotropy, evaluated at ray angles that are well sampled, is 3% at a radius of 1050km (depth of 150 km) and increases to 4% near 700km radius. At greater depth, the anisotropy appears to decrease somewhat, but owing to a paucity of deeper penetrating rays, resolution below 500km is weak. Recent analyses of Shearer [1994] and Song and Helmberger [1994] suggest that anisotropy is very weak, or nonexistent, in the outer 100km of the inner core. The ISC data are in general agreement with our model [*Shearer*, 1994], though Su and Dziewonski's [1994] analysis of the ISC data argue for a much lower level of anisotropy. Our model is also in general agreement with the model produced by Tromp [1993] from normal-mode observations, though our model suggests stronger anisotropy deep in the inner core where the modes begin to lose resolution. There is general agreement among seismologists that the anisotropy is strong, and that the symmetry axis is near (within about 10°) of the Earth's spin axis. Our best fitting axis is at 80°N, 170°E. However, the range of acceptable models include the spin axis, but only 4% of the possible range of symmetry axis directions.

The large amplitude (3–4%) of the anisotropy from about 200km to at least 600km depth into the inner core, and the fact that the symmetry axis lies near the spin axis have important implications for constraining possible mechanisms for producing the anisotropy. We analyze previously suggested mechanisms, and propose several new ones that could produce large-scale seismic anisotropy. The mechanisms that appear most plausible and can explain both the observed symmetry, and high strength of anisotropy over a large depth range, are all related to alignment of iron crystals in a strong toroidal, axi-symmetric magnetic field. If this is the case, it has important implications on the possible models for the geodynamo and, potentially, for the evolution of the core/geodynamo system. For example, it appears that some dynamo models, such as α^2 dynamos, could not have been operating at the time the anisotropy was acquired.

The very large degree of anisotropy inferred here from body-wave data is difficult to reconcile with the recent first-principle calculations of the level of anisotropy in hcp iron [*Stixrude and Cohen*, 1995]. According to their calculations, a 100% alignment of iron

crystals would come close, but would still underpredict our observations. This degree of alignment seems highly unlikely. Reconciling observations and theory is an important direction for future work.

In addition to anomalous travel times, Creager [1992] reported that the P'_{DF}/P'_{BC} amplitude ratios were systematically three times smaller for rays nearly parallel to the spin axis relative to those in other directions. Analysis of this strong signal is likely to remove some of the ambiguity of models constructed from travel times alone.

Chapter 3: The Core Mantle Boundary

3.1 Introduction

The Earth's interior was divided by Bullen [1949] into six distinct regions based on changes in seismic velocities as a function of depth (based on the models of Jeffrey's). If the F region, which represented a boundary layer of some sort at the base of the outer core, is neglected we are left with the following, simplified, picture of the Earth's deep interior. These five regions are the crust (or A region, from the surface to the top of the mantle), the upper mantle (or B region, from the base of the crust to the top of the transition zone at about 400 km depth), the transition zone (or C region, from 400-660km depth), the lower mantle (or D region, from 660-2900km depth), the outer core (or E region), and the inner core (or G region). If one assumes that a region of the Earth is homogeneous (in the chemical sense), then by utilizing the Adams-Williamson relationship (presented in Chapter 1) the gradient of incompressibility with pressure can be written as

$$\frac{d\kappa}{dp} = 1 - \frac{1}{g}\frac{d\phi}{dz} \qquad 3\text{-}1$$

where g is the gravitational acceleration, z the depth, ρ the density, κ the incompressibility, and $\phi = \alpha^2 - (4/3)\beta^2$ the so called "seismic parameter". When this parameter was calculated for the lower mantle and core, Bullen found $d\kappa/d\rho \approx 3$ for most of the lower mantle, except at the base of the mantle, where $d\kappa/d\rho \approx 1$. This suggested that the lower mantle was homogeneous to 2700km depth, but that below this there was a second region that was chemically distinct. As a result, Bullen separated his original "D region" into two regions: the D' region from 660-2700km depth, and the D" region from 2700km depth to the base of the mantle. This D" region is distinct seismically, as well as chemically from the rest of the lower mantle. Seismically, the D" region is characterized by changes in seismic velocity gradients from those typical in the rest of the lower mantle (where the gradients in P and S wave velocities change very little). In the terminology that we will be using here the D" region can be understood to define a region with anomalous seismic properties

at the base of the lower mantle, while the CMB can be understood to define the dynamical boundary between the core and the mantle.

The CMB has interested earth scientists continually for the last 30 years. This interest is primarily due to the importance that the properties of this region are thought to have on several important and related processes. The CMB is a boundary in many respects. At the CMB, there are dramatic changes in density, material properties (like chemistry, conductivity, and viscosity), and overall dynamics. This region separates the overlying, slowly convecting, crystalline mantle from the underlying liquid, rapidly convecting outer core. It also divides the Earth into two primary compositional regions, the silicate mantle above and the mostly iron core below. The jump in density across the CMB (nearly 4.4 g/cm^3) is even larger than the density contrast at the Earth's surface, a factor that, most likely, has a dramatic effect on the structure of the region as a whole. This region also separates the electrically conducting, fluid outer core, where the Earth's magnetic field is thought to be generated, from the insulating, solid mantle. There are some authors who have proposed that, at the pressure and temperature conditions present at the CMB, there could be chemical interactions between the silicates in the mantle and the liquid iron in the core [*Knittle and Jeanloz*, 1991]. Any lateral variations in electrical conductivity (from that of the overlying mantle) within this layer could have profound effects on the dynamics of the Earth's magnetic field.

The heat flux through this boundary is also thought to play an important role in mantle convection. In fact, the temperature at the top of D" is a critical parameter in determining whether a second boundary layer is needed in the mantle (in order to account for the total temperature change across the mantle). If this is the case, then convection in the mantle may be layered, with the second boundary layer (often proposed to be the 670km seismic discontinuity) acting as a barrier to mantle convection (and, in the same vein, as a barrier to subduction). If not, then convection in the mantle is thought to be whole mantle convection and subduction may continue into the lower mantle. This controversy has important implications for mantle dynamics and plate tectonics.

Finally, this region is thought to represent a highly dynamic region. In order to account for the relatively stationary position of hotspots at the Earth's surface, it has been proposed that the mantle plumes that they represent originate in the deep mantle, most likely at or near the CMB. This region may also represent a sink for the "dregs" of mantle convection. Because of the large density contrast across the CMB, it is thought that the colder, heavier material in the mantle convection process could accumulate at the bottom of the mantle as "anti-continents" in a manner similar to the accumulation of the lighter, continental crust trapped at the top of the mantle. With this in mind, it shouldn't be unreasonable to expect that there could be rather strong changes in composition and material properties in this region over all length scales, a point that we will return to later in the chapter. It is for this reason that a region originally thought to only be of interest seismologically (the D" region) has been the subject of a great deal of research in areas as widely varying as mineral physics, geomagnetism, geodesy, and geodynamics.

Interest in imaging the details of the seismic structure of the CMB developed soon after the region was discovered. In the late 1930's, a series of 1–D seismic models were proposed for this region [*Gutenberg and Richter*, 1939; *Jeffreys*, 1939]. While the details of these models are no longer of importance, they did include changes in the gradients of P and S wave velocities in the (soon to be named) D" region. The first attempt to determine the details of D" velocity structure was made by Alexander and Phinney [1966], who used spectral analysis of diffracted P waves to constrain the thickness and lateral variability of D" velocities. The use of diffracted waves removes the complication of trying to correct for the (relatively) unknown effects of mantle structure that lay above the region of interest (at least for the downgoing ray). However to utilize their technique they needed to have at least two stations at roughly the same azimuth from the earthquake which spanned a distance range of at least 20°, and the earthquake source needed to be quite large (they used a cutoff of 6.5 in magnitude). They modeled the spectra of these diffracted waves by assuming that the peaks and valleys in the spectra represented the transmission and absorption peaks of waves that had traveled in the "waveguide" of the CMB. Their analysis showed that the average P–wave velocity at the core-mantle boundary changed geographically and, at least at

the scale that they could resolve, there was very little dispersion inherent in their observations. This implied that there was very little overall vertical change in the ray parameter (v/r) for rays turning in D", at least in a global sense. Unfortunately, they could not determine the thickness of this boundary layer except to say that this region was less than 160km thick, on average.

In an attempt to increase the resolution of the work by Alexander and Phinney [1966], Johnson [1969] used short-period P-wave travel times recorded at the extended array of the Tonto Forest Seismological Observatory in Arizona to image D". In the observations he collected, there was a clear change in the slope of the travel time curves observed at the array near 90° epicentral distance. This supported the concept of an anomalous velocity structure at the base of the CMB, but the details of this structure were not well resolved by the data in his study. There was also a much larger degree of scatter in the data beyond 90° than was found in the data for closer distance ranges. Initially it was thought that this might represent the effects of a complicated velocity structure near the CMB (which gave rise to a triplication or series of triplications in the travel times), however, after correcting the data for the effects of the core [*Phinney and Alexander*, 1966], it was determined that a more likely source for the remaining scatter was the presence of lateral variations in the structure of the D" on a global scale, a possibility that was also mentioned by Alexander and Phinney [1966].

Following Johnson, several authors used observations of PKP precursors to study the structure of the Earth's core. Bolt [1962] interpreted these precursors to observations of PKP_{DF} phases in the distance range $120° < \Delta < 143°$ as resulting from refraction at the outer boundary of a proposed transition layer between the inner and outer cores. This hypothesis led to an explosion of models of this "ICB transition zone" [*Adams and Randall*, 1964; *Bolt*, 1964; *Buchbinder*, 1971; *Ergin*, 1967; *Huseby and Madariaga*, 1970; *Qamar*, 1973]. However, the later papers by Buchbinder [1971] and Qamar [1973] showed that Bolt's original hypothesis didn't fit the observed amplitudes of the precursors. Instead, they suggested that these precursors were the result of reflections from a small velocity discon-

tinuity at the top of this ICB transition layer.

Haddon and Cleary [1974] and King et al. [1974] proposed that these precursors were, in fact, the result of scattering of the PKP wavefront as it moves through the D" region. They used a scattering theory developed by Haddon and data collected at the NORSAR and Warramunga seismic arrays to examine and model the amplitude variations within the precursor wavetrain. The variations in the amplitude and frequency content of these precursors can be used to determine the thickness and correlation distance for the scatterers (which gives an idea of the minimum scale of variations in CMB structure), factors that could have important implications for many current discussions of chemical alteration and accumulation of material at the CMB from mantle convection. They found that the precursors observed from worldwide events could be explained by variations of about 1% in density and elastic parameters in a layer less than 200km thick at the base of the mantle. The correlation distance that best fit their observations was approximately 30km, so it is entirely reasonable, based on these models, that high wavenumber variations in seismic and material properties exists in D". The existence of such high wavenumber structure in D" could have important implications for interpretations of current CMB P and S wave velocity models, a point that we will return to later in this chapter. With these models they were able to not only explain the travel times and maximum amplitudes of the observed precursors as a function of distance, but also such diverse factors as the temporal variations of amplitude and slowness within the precursor wavetrains, the lack of signal coherence within the arrays used, and the variability of observations for different event station geometries. None of these latter factors could be explained by the alternative, ICB transition zone, hypotheses.

More recently, there has been a renewed interest in studying the variations in seismic properties of the CMB at a regional level using the travel times of P and S phases (core transmitted, diffracted and reflected phases have all been used). For example, Wyssession et al. [1992] used diffracted P and SH phases to model the structure of the CMB. As with the spectral analysis of Alexander and Phinney [1966], long period waves were used, and

measurements of travel times to several stations at similar azimuths were used to determine the average slowness (or average velocity) of the CMB along a series of "profiles". They found that there were regions where the P and S-velocity had the same sense (i.e. highs in P-velocity corresponding to highs in S-velocity and vice-versa), and that there were regions where the P and S-velocities had the opposite sense(i.e. highs in P-velocity corresponding to lows in S-velocity and vice-versa). In a similar vein, Garnero and Helmberger [1993] used travel times of S and SKS phases to study S wave variations in D" under the central Pacific, and, more recently, they have used differential travel times of diffracted S (or S_d), S_dKS, SKS_d and SKS to study the same region [*Garnero and Helmberger*, 1993]. In both studies, the observations were consistent with each other. This observation of regional coherence and global variation led to a recent study by Wysession et al. [1994], in which they used differential travel times of ScS and S phases to study the CMB in the region beneath Australia and Indonesia. They obtained a high resolution model of the CMB that was consistent with the earlier results they obtained for the same region using diffracted phases but showed that the structure in the CMB can be highly variable over relatively small distance scales. They also found, in comparing their diffracted P and S results globally, that while there are areas where P and S velocity variations correlate well, there are other areas where they correlate very poorly (or anti-correlate quite well). Recently, Rodgers and Wahr [1993] reviewed the status of current attempts [*Creager and Jordan*, 1986; *Doornbos and Hilton*, 1989; *Morelli and Dziewonski*, 1987] to image D" using ISC times. They found that the existing datasets of catalog times were not sufficient for properly imaging D".

3.2 Observations

In this part of our study, the observations that we analyze are the same phases (P'_{DF}, P'_{AB}, and P'_{BC}) that were used in modeling inner-core anisotropy in Chapter 2. However, if one is attempting to model CMB structure, then the best phase pairs to use are not the same as those used to study inner core anisotropy. In studying the inner core, we specifically chose to concentrate on the differential travel time pair P'_{BC}–P'_{DF} because these two phases were quite close to each other throughout most of the mantle and the core-mantle

boundary. In order to study the anisotropy of the inner core at greater depths, however, we used the differential travel time pair P'_{AB}–P'_{DF}. In interpreting these observations, we were very careful to keep in mind the potential effects of CMB structure on these differential travel times. In studying the structure of the CMB, however, we concentrate on the differential travel time pairs P'_{AB}–P'_{BC} and P'_{AB}–P'_{DF}, since the P'_{AB} phase has a much more grazing incident angle with the CMB than either the P'_{DF} or P'_{BC} phases (see the ray diagram in Figure 2-1 for an example of this). As a result, of these three phases, the P'_{AB} phase is, on average, three times more sensitive to D" structure than either P'_{DF} or P'_{BC}. In Chapter 2 we showed that the inner core can cause huge (up to 6 s) differential travel time anomalies, but that these large residuals were always confined to paths with a P'_{DF} ray orientation within 40° of the spin axis direction. The rms of P'_{BC}–P'_{DF} residuals for ray angles exceeding 40° is only 0.5 s, which suggests that inner core structure has a fairly small effect on the P'_{DF} times.

There are basically two approaches that could be taken to this problem. One would be to determine which P'_{AB}–P'_{DF} observations are strongly effected by the inner-core anisotropy that we studied in Chapter 2 and then remove them from further analysis. The second would be to correct the data for our preferred inner-core anisotropy model, thereby reducing the effects of inner-core anisotropy from the data. In order to avoid the potential pitfalls of overfitting data with small ξ values that have small P'_{AB}–P'_{DF} residuals, and then using the resulting large negative P'_{AB}–P'_{DF} residual with respect to our AXSYM model to determine a model for D", we have chosen to remove all of the data with ξ values of 40° or less from the analysis of D" (those data that are strongly effected by the anisotropy of the inner core). With either approach there is the danger of mapping lower mantle structure into the CMB region, so the resulting models should be viewed with some cautious scepticism. two other potential sources of bias that we have not attempted to correct in our analysis are earthquake mislocations and the structure of subducting slabs beneath the earthquake sources [*Helffrich and Sacks*, 1994].

3.3 Data Description

The data analyzed in this chapter are described in detail in Chapter 2. Of the 322 P'_{AB}–P'_{BC} and 1061 P'_{AB}–P'_{DF} differential travel times measured in our original dataset, we have used 300 P'_{AB}–P'_{BC} and 870 P'_{AB}–P'_{DF} differential travel time residuals (with respect to PREM) from hand-picked differential travel times of seismograms from the GDSN, ASN, CALNET, and GSN arrays in our analysis of D". In choosing differential travel times for this study, we restricted the dataset to only times of high quality (quality 1 and 2) and, in the case of the P'_{AB}–P'_{DF} times, high ξ value ($\xi > 40°$). See section 2.2 for a discussion of the networks, the procedure used to measure differential travel times of these phases, quality factors used and accuracy of the picks.

The geographic coverage of this dataset at the CMB can be seen in Figure 3-1. In the future, these phases could be combined with the differential travel times used in this study (in particular we would like to use PcP–P differential travel times for a study such as this) in order to obtain a much more highly constrained model of D" P–wave velocity structure, however, we will limit the scope of this study to actually testing whether or not these phases can be used to determine a preliminary map of D" P–wave velocity structure. The merging of this dataset with other D" sampling P phases will be left to a future date.

In removing the data values for which the P'_{DF} ray has a ξ value of 40° or less, only 95 P'_{AB}–P'_{DF} times were discarded from the dataset. The remaining differential travel time residuals have a mean value of 0.43 s and a standard deviation of 1.01 s. Appendix A discusses the fit of PREM to these data. The mean and standard deviation of the P'_{AB}–P'_{DF} and P'_{AB}–P'_{BC} residuals separately are: $\bar{x} = 0.53$, $\sigma = 1.05$ and $\bar{x} = 0.09$, $\sigma = 0.79$ respectively. The effects of inner core anisotropy on this dataset appear to be minimal. The P'_{AB}–P'_{DF} data show a much higher average value, which may be the result of a misfit of PREM to average velocities in the inner core. Overall, the P'_{AB}–P'_{BC} data are better fit by PREM than the P'_{AB}–P'_{DF} data. Although there does appear to be a misfit of PREM to the

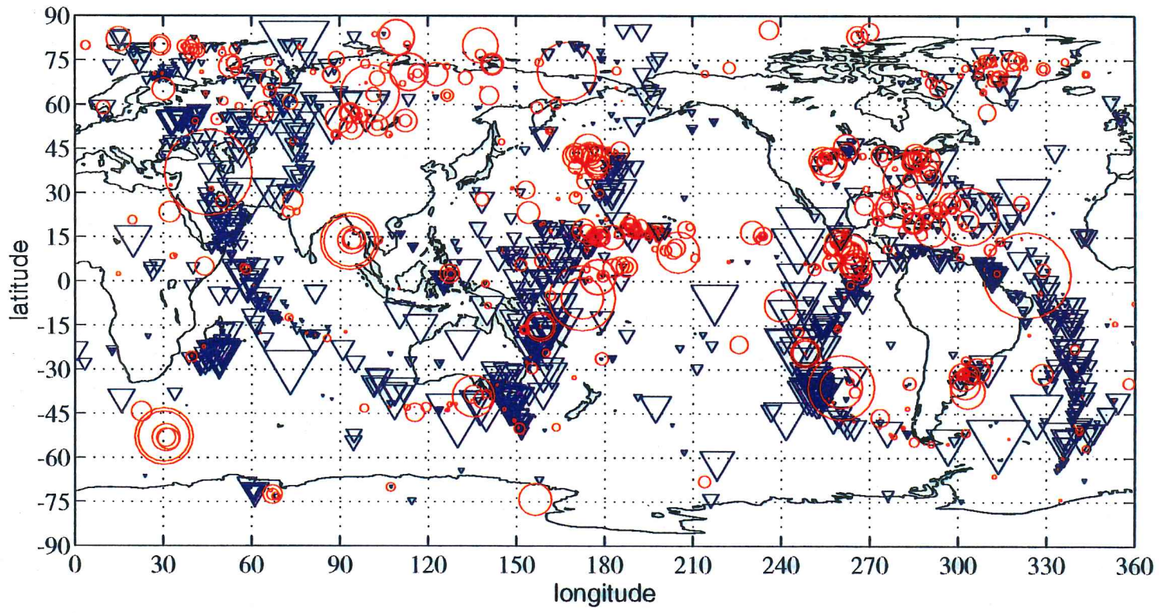

Figure 3-1: A plot of the data used in the study of D" at the CMB interaction points of the P'_{AB} rays. The inverted triangles show positive residuals with respect to PREM, the circles negative residuals with respect to PREM. Symbols with a radius of 3° have a magnitude of 1 second (i.e. a symbol with a diameter of 30° represents a 5 second residual).

P'_{AB}–P'_{DF} times, it is small enough that we feel comfortable using PREM as a starting model for our inversion.

The scatter in the data (92% of the residuals magnitudes < 2.0 s) is probably best explained by structure in the lower mantle for several reasons. First, the lowermost mantle is where the rays are most separated from each other. Second, from previous studies of the lower mantle, the lowermost mantle is where the magnitude of perturbations to average earth models (like PREM) are known to increase. Finally, the P'_{AB} rays are very sensitive to structure in the lowermost mantle, especially the D" region, where they are nearly core grazing. We do not believe that it is likely that residuals of this size could be caused by structure in the inviscid, liquid outer core, although this study does not test this hypothesis in any way. It is entirely reasonable to believe that travel time anomalies of the magnitude observed in this study could be explained by structure in the CMB, as we will be proposing here, but it should be remembered that the P'_{AB} phase is several hundred kilometers from either the P'_{BC} or P'_{DF} rays throughout the lowermost mantle, so the velocity anomalies that we will estimate represent average anomalies through the lowermost mantle. We will present our results as travel time perturbations integrated along radial paths through a 200km thick D" layer. If the region in the lower mantle that is causing the differential travel time residuals is considerably thicker or thinner than this, the model's velocity perturbations can be adjusted accordingly.

A further complication that we have not accounted for is the effect of inner core heterogeneity. While we have reduced the effects of inner-core anisotropy by limiting the range of ξ values of the P'_{DF} phases, the effects of inner-core heterogeneity, if any, cannot be removed in this manner. Only a sufficient number of crossing paths or a larger number of P'_{AB}–P'_{BC} times can remove the potential effects of inner-core heterogeneity. In this dataset we have only a small number of crossing paths and a small number of P'_{AB}–P'_{BC} times, so our model should be viewed with some scepticism. However, as can be seen in Figure 3-2, the effects of inner core heterogeneity are rather small when compared to the

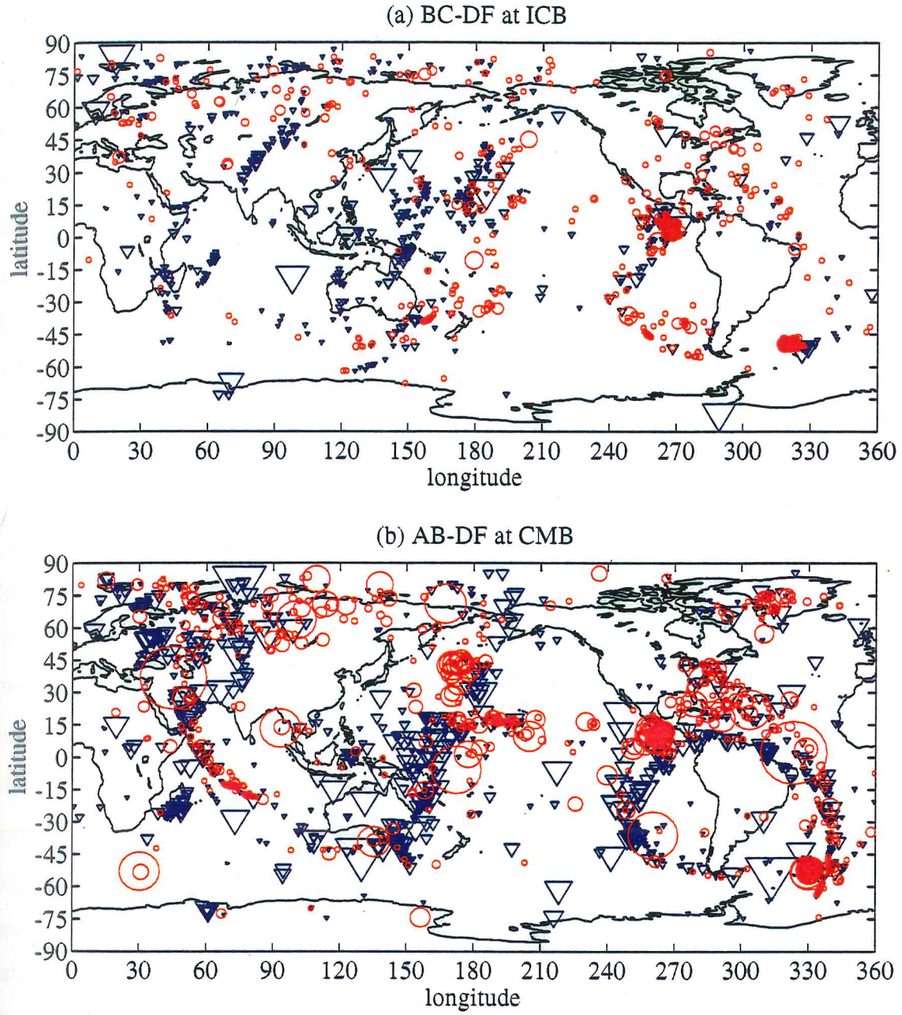

Figure 3-2: (a) A plot of the P'_{BC}–P'_{DF} residuals to PREM at the ICB interaction points of the P'_{DF} rays. The circles represent negative residuals, the inverted triangles positive residuals. The symbols are, on average, much smaller than those plotted in (b), which shows the P'_{AB}–P'_{DF} residuals plotted at the CMB interaction points of the P'_{AB} rays. In both (a) and (b) the scale is the same as in Figure 3-1 (i.e. 30° diameter symbol represents a 5 second residual).

effects of D". The top panel shows all of our P'_{BC}–P'_{DF} data with $\xi > 40°$ (i.e. those unaffected by the anisotropy in the inner core) plotted at the ICB interaction points of the P'_{DF} rays. These residuals can best be explained as the result of the effects of heterogeneity in the inner core, since the P'_{BC} and P'_{DF} rays are very close to each other throughout most of the mantle and core. The bottom panel shows our corresponding P'_{AB}–P'_{DF} data (again only those data where $\xi > 40°$) plotted at the CMB interaction points of the P'_{AB} rays. It should be apparent that the contributions are, on average, very small from inner core heterogeneity. In contrast, the signal seen in the P'_{AB}–P'_{BC} and P'_{AB}–P'_{DF} data is, on average, 2-3 times larger.

3.4 Modeling

We invert the differential travel time pairs P'_{AB}–P'_{BC} and P'_{AB}–P'_{DF} for a smooth model of lateral variations in the velocity of D". Each of our observations is associated with 4 separate interaction points on the CMB, the entry and exit points of the P'_{AB} ray and the corresponding entry and exit points of either the P'_{DF} or P'_{BC} ray. Because of their near core-grazing incidence angles at the CMB, P'_{AB} rays are, on average, about three times more sensitive to D" structure than either the P'_{BC} ray or the P'_{DF} ray. We have chosen to follow a simple modification of the stochastic inversion procedure used by Creager and Jordan [1986]. In the stochastic inversion procedure, the N-dimensional vector ($\vec{\Delta\tau}$) of the N observed differential travel-time residuals are assumed to be a sample of a stochastic process (one could call it the "data process"). The model itself is represented by vertical travel time anomalies, $\delta\tau(\Omega)$, as a function of position $\Omega = (\theta,\phi)$, predicted for a change in velocity, $\delta v(r,\Omega)$, with respect to PREM on a spherical shell above the CMB

$$\delta\tau(\Omega) = -\int_{R}^{R+200} \frac{\delta v(r,\Omega)}{v_0^2(r)}\, dr \qquad 3\text{-}2$$

where v_0 represents the PREM velocity and R the radius of the CMB. The theoretical dif-

ferential travel time residuals can be decomposed into 4 terms, due to the velocity anomalies at the entrance and exit points of the first and second phase (where the differential travel time anomaly is calculated as phase$_2$–phase$_1$). Then the j–th differential travel time residual can be written as

$$\Delta\tau_j = \gamma(p_j^2)\,[\delta\tau(\Omega_j^{2,in}) + \delta\tau(\Omega_j^{2,out})] - \gamma(p_j^1)\,[\delta\tau(\Omega_j^{1,in}) + \delta\tau(\Omega_j^{1,out})] \qquad 3\text{-}3$$

where p is the ray parameter of the phase in question. In this notation, the superscript 2 is used to represent the ray parameter and interaction point positions of the P'$_{AB}$ phase, while the superscript 1 is used for either the P'$_{BC}$ or P'$_{DF}$ phase, depending on which differential travel time pair is being represented by the j–th differential travel time residual. The subscript j is used to denote the j–th observation, and the superscripts "in" and "out" on the position, Ω, are used to denote the ingoing and outgoing interaction points for a given ray, respectively. The quantity γ (above) is defined as

$$\gamma(p) = \frac{1}{200} \cdot \int_R^{R+200} \frac{\eta}{\sqrt{\eta^2 + p^2}}\, dr \qquad 3\text{-}4$$

where η is defined as

$$\eta(r) = \frac{r}{v(r)} \qquad 3\text{-}5$$

for the PREM model. From equation 3-4, one can see that γ is a dimensionless function of ray parameter only, which equals 1 for vertical paths (such as P'$_{DF}$) and reaches values as large as 6 for P'$_{AB}$ at large epicentral distances. This function simply maps the perturbations to the predicted PREM vertical travel times (the $\delta\tau$ values on the right side of equation 3-3) into observed differential travel time perturbations. The observed differential travel time residuals, then, can be written as

$$\Delta\tau_j = B_j(\Omega) \cdot \delta\tau(\Omega) = \int_0^{\pi}\int_0^{2\pi} B_j(\theta,\phi)\,\delta\tau(\theta,\phi)\sin\theta\, d\phi d\theta \qquad 3\text{-}6$$

where $B_j(\Omega)$ is defined as

$$B_j(\Omega) = \gamma(p_j^2)\,[\delta(\Omega-\Omega_j^{2,in}) + \delta(\Omega-\Omega_j^{2,out})] - \gamma(p_j^1)\,[\delta(\Omega-\Omega_j^{1,in}) + \delta(\Omega-\Omega_j^{1,out})] \qquad 3\text{-}7$$

and $\delta(x)$ is the dirac delta function. Following the stochastic inversion procedure presented by Creager and Jordan [1984], a covariance for the model (which is expressed as a covariance of the model with position $\hat{\mathbf{r}}$ on the unit sphere) is specified before the inversion is performed. The model that best fits the data with a covariance closest to the chosen covariance value is then determined by the stochastic inversion procedure. The equation that is used to perform the inversion for a given value of the model covariance matrix, $\mathbf{C}_{ss}(\hat{\mathbf{r}}, \hat{\mathbf{r}}')$, is

$$\delta\tau(\Omega) = \boldsymbol{C}_{ss} \cdot \boldsymbol{B}\,(\boldsymbol{B} \cdot \boldsymbol{C}_{ss} \cdot \boldsymbol{B} + \alpha \boldsymbol{C}_{nn})^{-1} \overrightarrow{\Delta\tau} \qquad 3\text{-}8$$

where $\mathbf{C}_{nn}$ represents the diagonal matrix of estimated uncertainties in the data (for this experiment, $\mathbf{C}_{nn} = \boldsymbol{I}$). Following Creager and Jordan's procedure, the $\mathbf{C}_{ss}$ "smoothing operator" is chosen to be the product of a real value function with itself

$$\mathbf{C}_{ss}(\hat{\mathbf{r}}_1, \hat{\mathbf{r}}_2) = \oint_{S(1)} \mathbf{g}(\hat{\mathbf{r}}_1, \mathbf{r})\,\mathbf{g}(\hat{\mathbf{r}}_2, \mathbf{r})\,d\,\Omega(r) \qquad 3\text{-}9$$

where S(1) is the unit sphere. If a spherical gaussian function of the form

$$\mathbf{g}(\hat{\mathbf{r}}_1, \hat{\mathbf{r}}_2) = \frac{\exp[\kappa(\hat{\mathbf{r}}_1 \cdot \hat{\mathbf{r}}_2)]}{4\pi i_0(\kappa)} \qquad 3\text{-}10$$

is chosen for the smoothing operator, where $i_0(x) = \sinh x / x$ is a spherical modified Bessel function, then the covariance of the model can then be rewritten as

$$\mathbf{C}_{ss}(\hat{\mathbf{r}}_1, \hat{\mathbf{r}}_2) = \frac{i_0(\kappa b)}{4\pi i_0^2(\kappa)} \qquad 3\text{-}11$$

where $b = \left| \hat{\mathbf{r}}_1 + \hat{\mathbf{r}}_2 \right|$. Note that $\mathbf{C}_{ss}$ is arbitrarily scaled so that the integral over the unit sphere of $\mathbf{C}_{ss}(\hat{\mathbf{r}}_1, \hat{\mathbf{r}}_2)$ equals one. This is the form of the autocorrelation function that we have chosen for our inversion. Note that the form of the spherical gaussian allows us to specify the "half-width" of the gaussian as

$$\frac{\exp\left[\kappa\cos\left(\Delta_{1/2}\right)\right]}{\exp\left[\kappa\right]} = \frac{1}{2} \qquad \textit{3-12}$$

which, when solved for $\Delta_{1/2}$ gives rise to the relation

$$\Delta_{1/2} = \operatorname{acos}\left(1 - \frac{\ln(2)}{\kappa}\right) \qquad \textit{3-13}$$

In our model, since we do not feel that our data sample the CMB uniformly enough at scale lengths much smaller than 70° or so (see Figure 3-1), a value of $\kappa = 4$ has been chosen, giving a half-width of this spherical gaussian smoothing operator of 34°. The resulting model will then have structure on approximately the same length scale as we can resolve at the CMB using the data from this study.

3.5 Discussion

The model resulting from our inversion of PKP differential travel time residuals for D" P-wave velocity structure is shown in Figure 3-3. The two parameters that can be varied in the inversion are κ and α (see equations 3-8, 3-9, and 3-10). For the reasons given above, we set κ=4. We chose α (see equation 3-8) to equal 10^{-4} times the largest eigenvalue of the NxN matrix $B \cdot C_{SS} \cdot B$. This choice of the trade-off parameter α produces a model with 32 degrees of freedom. For comparison, a spherical harmonic expansion to degree and order 5 would have 36 degrees of freedom. Even with the small number of free parameters, this model explains 46% of the variance in our observations. The model is given as predicted vertical travel time residuals through D". These vertical travel time residuals through D" can be converted to velocity anomalies if a specific thickness for D" is chosen. Choosing a thickness of 200km for D", we obtain peak to peak velocity perturbations to PREM in our

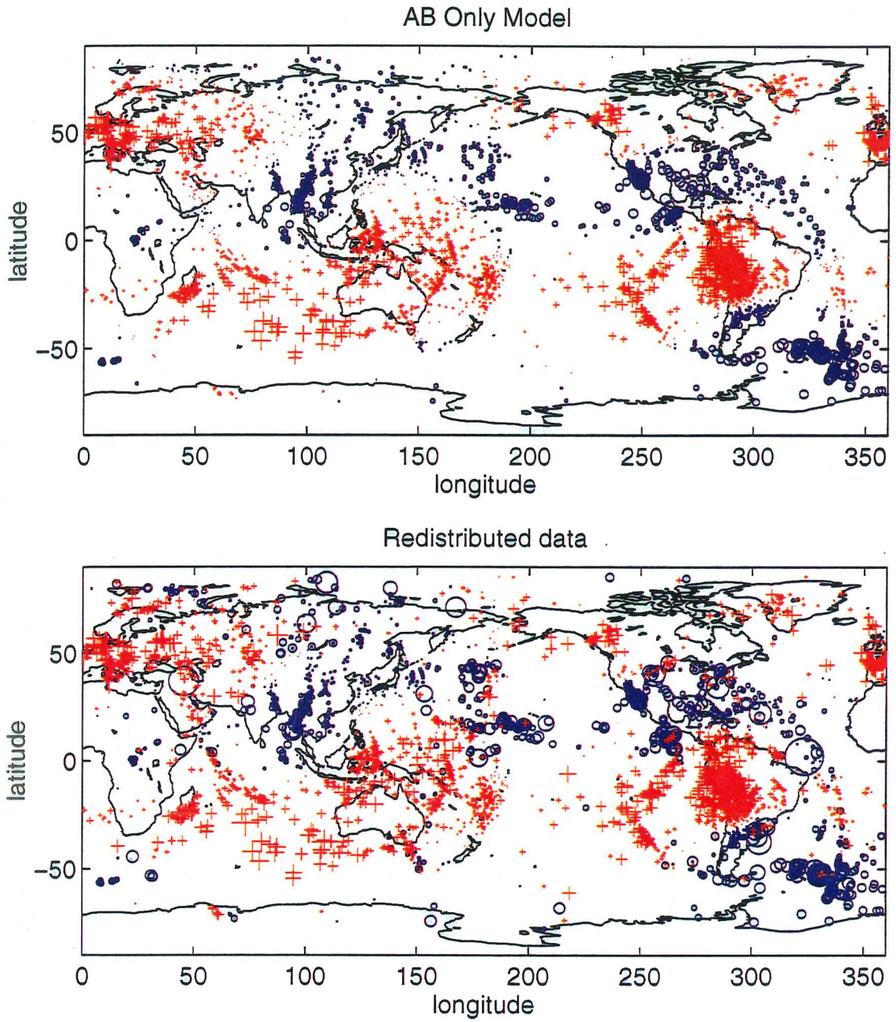

Figure 3-3: (a) A map showing the vertical travel time residuals predicted by our model for D" P-wave velocity anomalies at each of the P' interaction points and (b) the residuals in our dataset redistributed according to the predictions of our model. In both of these figures a plus sign represents a positive residual and a circle represents a negative residual. The scale in these figures is such that a 1 second residual appears as a 3° diameter symbol (or 15° for a 5 second residual).

model of ~3%, which give rise to peak to peak travel time perturbations of ~1.5 seconds for vertical ray paths through D". At the largest scales, the model appears to have a fairly distinct Degree 3 and Order 0 structure to it, with distinct bands of fast, then slow, then fast, and finally slow anomalies dominant in the data as one moves from south to north in the map view.

There are regions of this model that correlate quite well with regional studies from previous authors using diffracted P. For example, the large positive region in our model beneath Asia is a well documented feature that has been found by several recent studies of diffracted P and S [*Wysession and Okal*, 1989; *Wysession et al.*, 1992], as is the slow region beneath Alaska, the slow regions beneath Europe and North Africa, and the gradient from slow times under Indonesia to fast times under Southeast Asia [*Wysession and Okal*, 1989; *Wysession et al.*, 1992]. Unfortunately, the coverage of the diffracted P studies is not very extensive (the well resolved regions are predominantly limited to the regions mentioned above). Comparison with various P wave mantle models is also not very satisfactory, since most of the P wave mantle models lack much resolution of the D" region [*Pulliam and Stark*, 1993]. As an attempt at comparison with one of the few lower mantle models that are in the literature, we correlated the predicted velocity anomalies from our model with those predicted for LO2.56 [*Dzeiwonski*, 1984] at the same points in D". The results were not very encouraging. The LO2.56 model correlated with our model at a level of -0.2 and, when a variance reduction for our dataset was calculated using the predicted times for our dataset of the LO2.56 model, it actually increased the variance in our dataset by about 6%. This discrepancy between the values predicted by LO2.56 and our observations may, in fact, be due to the lack of resolution problem. If LO2.56 has little or no resolution in the lowermost mantle, then the effect of their parametrization would be to downward continue the model from a level higher in the lower mantle with little or no change. If the D" region is really radically different (dynamically speaking) than the region of the mantle above it, then there is little reason to believe that there would necessarily be a correlation between the velocity structures in D" and those in the lower mantle above D". As a result, to make comparisons with P-wave models, we need to find other P-wave models that have high res-

olution within the D" region, and, to date, the only models that have adequate resolution of D" are the diffracted P models.

As is apparent in Wyssession's [1989] recent comparison of diffracted S and diffracted P models of D" structure, the P and S velocities in the D" region correlate well in some areas and poorly in others. This regional difference between P and S models may prove to be one of the important constraints that seismology can provide on the degree of thermal/compositional changes in D". It is likely that the effects of thermal and compositional changes on seismic wavespeeds are quite different for P and S waves, and that this sort of difference could be called into effect to explain regional differences in correlations between P and S velocities in D". First, however, adequate models of P and S velocities in this region must exist. The models of S wave velocities in D" are much better constrained than those of P waves, mainly because the ScS phase on the transverse component is a very strong phase, while the equivalent P phase (PcP) is rather weak. As a result, accurate ScS–S picks have recently been made for large datasets of digital long period waveforms. This phase pair has been used recently to estimate the S velocity structure of D" both regionally [*Wysession et al.*, 1994] and globally [*Woodward and Masters*, 1991], and it has also been used to constrain the D" S velocity structure of two recent whole mantle tomographic models, SH.10C.17 [*Su and Dziewonski*, 1994] and S12_WM13 [*Masters et al.*, 1992].

Using a standard scaling ($d(\ln\beta)/d(\ln\alpha) = 0.5$) we calculate the vertical P-wave travel times anomalies predicted for these S models through a 200 km thick D" boundary layer at each of the ray sampling points. The scaled S models reduce the variance in our data by 8% (SH.10C.17) and 6% (S12_WM13), while the correlation coefficients of each of the models with our model are 0.28 and 0.27, respectively. This shows that the trend observed by Wyssession [1989] in diffracted P and diffracted S is also apparent in the differential PKP and differential ScS–S times, that there is very poor correlation (worldwide) between lateral variations of D" P and S velocity anomalies. This same trend can also be seen at a local level when our PKP model beneath Australia is compared with the ScS–S model of Wysession [1994]. While there is a large area under Indonesia, the Pacific, and

Australia where the two models correlate well, there is also a region south and west of Australia where the S model is fast and our P model remains slow.

3.6 Conclusions

We have inverted 1383 PKP differential travel times for a model of P velocity structure in the D" region. Assuming a thickness to D" of about 200km, the resulting model has peak to peak velocity perturbations in D" (with respect to PREM) of ~3%. Previous attempts to determine the large-scale velocity structure near the CMB [*Creager and Jordan*, 1986; *Doornbos and Hilton*, 1989; *Morelli and Dziewonski*, 1987; *Rodgers and Wahr*, 1993] have relied on ISC observations. Our observations provide a global coverage that approaches the coverage of these studies and greatly reduces the problems associated with relying on bulletin reported travel times, especially for the P'_{AB} phase, which is Hilbert transformed. While comparison of our results from those obtained by several recent regional studies of the CMB region [*Grand*, 1994; *Wysession et al.*, 1994; *Wysession and Okal*, 1989; *Wysession et al.*, 1992] are encouraging, the predictions of global models for this region, in particular a lower mantle P velocity model (LO2.56) and two recent mantle S velocity models (S12_WM13 and SH.10C.17), show a poor correspondence with both our model and our observations. While the dataset presented here demonstrates that there are regions of the lower mantle with scale lengths of thousands of kilometers that have consistently high (or low) velocities of a percent or more (with respect to PREM), a consensus has yet to be reached for the details of a large-scale P-velocity model for the CMB region. We have demonstrated the success of this technique and that the solution to the problem of imaging the deepest mantle will come from a combination of analysis of the data collected for this study and other similar studies of large, high quality, datasets. Comparison of the resulting models of lateral variations in P and S velocities, when combined with the results of laboratory analysis of material properties at CMB pressures and temperatures, should then allow for the determination of the degree to which the lateral variations in wavespeeds are caused by changes in temperature or composition or both.

Chapter 4: Future Work

While we are confident that, at least to first order, we have determined the variations of the level of anisotropy with depth in the inner core, this study does not answer a number of interesting questions. First, is there a heterogeneity in the anisotropy within the inner core? This question could have a number of important implications for some of the conclusions drawn at the end of Chapter 2. If there is heterogeneity in the anisotropy of the inner core, then the picture of the relationship between the inner-core anisotropy and the geodynamo may not be as simple as we have explained it here. Second, could these observations be used to constrain the scale of heterogeneity in the inner core? As they are presented in this study, we do not have enough information to separate the effects of the CMB and lower mantle from the effects of any aspherical velocity structures (aside from anisotropy) that may exist in the inner core. An analysis of the new P'_{BC}–P'_{DF} times, however, may shed new light on this problem because their contamination from D" is small. And finally (for the inner core), what do the amplitude ratios of these phases have to say? In this study we have explicitly avoided analysis of the amplitude data for the PKP waveforms, but the amplitude ratios and their variations with respect to parameters like ξ may have an important role to play in determining the fine structure of the inner core. In the future, as more data are collected from regional arrays, we will be able to study localized regions of the inner core utilizing the techniques presented here in order to determine answers to such questions as: (1) is the axis of symmetry of the anisotropy really constant laterally and with depth? (2) what are the scale lengths of heterogeneity in the inner core? and (3) what happens to the anisotropy as one nears the inner core boundary. Needless to say, the questions about the inner core are far from answered.

A number of interesting questions also remain with respect to structure in D". Our current model is not necessarily the best model for lateral variations of P-wave velocities in D". In the future it should be possible to take this PKP dataset and combine it with observations of other core sampling phases (like PcP) in order to overcome some of the non-

uniqueness inherent in the PKP differential travel times. Specifically, in the near future, we plan on combining this study with a study of variations of PcP–P differential travel times in order to get the benefits of both datasets (increased ray coverage in the PKP data and a more unique dataset in the PcP–P times). If a good model of the lateral variations in P-wave velocities in D" can be constructed in such a fashion, it should have an important role to play in determining the processes that are acting to cause the observed variations in material properties near the CMB.

In light of the new datasets and improved instrumentation available, I also believe that several old techniques deserve revisiting. There were several techniques developed (with respect to arrays, for example) in order to determine the fine structure of the CMB in the late 60's and early 70's, but the computer power, data, and instrumentation were not there do go with the theory. With continuous, broad-band data accumulating at an ever increasing rate from a wide variety of sources (from regional arrays to global arrays to temporary deployments of instruments in odd places), it is now possible to revisit some of these techniques and determine if the prospects for obtaining answers to the existing questions about the CMB (as an example, what is the spectrum of heterogeneity at the CMB? Are the present disagreements between P and S models, or with different S and different P models, just a matter of spatially aliasing a CMB with a great deal of fine structure because of differences in sampling or is there really a physical explanation that we need to obtain to try to answer based on these differences?).

References

Adams, R.D., and M.J. Randall, The fine structure of the Earth's core, *Bulletin of the Seismological Society of America*, *54*, 1299, 1964.

Ahrens, T.J., Equations of state of iron sulfide and constraints on the sulphur content of the Earth, *Journal of Geophysical Research*, *84* (B3), 985-998, 1979.

Aki, K., and P.G. Richards, *Quantitative seismology; theory and methods*, 932 pp., W.H. Freeman and Co., San Francisco, Calif., 1980.

Alexander, S.S., and R.A. Phinney, A study of the core-mantle boundary using P-waves diffracted by the Earth's core, *Journal of Geophysical Research*, *71* (24), 5943-5958, 1966.

Anderson, W.W., B. Svendsen, and T.J. Ahrens, Phase relations in iron-rich systems and implications for the Earth's core, *Physics of the Earth and Planetary Interiors*, *55* (3-4), 208-220, 1989.

Bhattacharyya, J., P. Shearer, and G. Masters, Inner core attenuation from short period PKP(BC) versus PKP(DF) waveforms, *Geophysical Journal International*, *114* (1), 1-11, 1993.

Bolt, B.A., and S. Gutenberg, Early PKP observations, *Nature*, *196*, 122, 1962.

Bolt, B.A., The velocity of seismic waves near the Earth's center, *Bulletin of the Seismological Society of America*, *54*, 191, 1964.

Bolt, B.A., The constitution of the core-seismological evidence, *Philosophical Transactions of the Royal Astronomical Society*, *306* (1492), 11-20, 1982.

Brown, J.M., T.J. Ahrens, and D. Shampine, Hugoniot data for pyrrholite and the Earth's core, *Journal of Geophysical Research*, *89*, 6041, 1984.

Buchbinder, G.G.R., A velocity structure of the Earth's core, *Bulletin of the Seismological Society of America*, *61*, 429, 1971.

Bullen, K.E., Compressibility-pressure hypothesis and the Earth's interior, *Monthly Notes of the Royal Astronomical Society, Geophysical Supplement*, *5* (9), 355-368, 1949.

Bullen, K.E., The rigidity of the Earth's inner core, *Annales Geophysique*, *11* (1), 53-64, 1953.

Choy, G.L., and P.G. Richards, Pulse distortion and Hilbert transformation in multiply reflected and refracted body waves, *Bulletin of the Seismological Society of America*, *65* (1), 55-70, 1975.

Cormier, V.F., Inner core structure inferred from body waveforms (abstract), *EOS Transactions of the American Geophysical Union*, *75*, 67, 1994.

Cormier, V.F., and G.L. Choy, Seismic velocities and attenuation at the inner core boundary (abstract), *EOS Transactions of the American Geophysical Union*, *67*, 311, 1986.

Creager, K.C., Anisotropy of the inner core from differential travel times of the phases PKP and PKIKP, *Nature*, *356* (6367), 309-314, 1992.

Creager, K.C., and T.H. Jordan, Slab penetration into the lower mantle, *Journal of Geophysical Research*, *89* (B5), 3031-3049, 1984.

Creager, K.C., and T.H. Jordan, Aspherical structure of the core-mantle boundary from PKP travel times, *Geophysical Research Letters*, *13*, 1497-1500, 1986.

Cummins, P., and L.R. Johnson, Short-period body wave constraints on properties of the Earth's inner core boundary, *Journal of Geophysical Research*, *93*, 9058-9074, 1988.

Doornbos, D.J., The Anelasticity of the inner core, *Geophysical Journal of the Royal Astronomical Society*, *38* (2), 397-415, 1974.

Doornbos, D.J., and T. Hilton, Models of the core-mantle boundary and the travel times of internally reflected core phases, *Journal of Geophysical Research*, *94*, 15741-15751, 1989.

Dzeiwonski, A.M., Mapping the lower mantle: Determination of lateral heterogeneity in P velocity up to degree and order 6, *Journal of Geophysical Research*, *89*, 5929-5952, 1984.

Dziewonski, A.M., and D.L. Anderson, Preliminary Reference Earth Model (PREM), *Physics of the Earth and Planetary Interiors*, *25*, 297-356, 1981.

Dziewonski, A.M., and F. Gilbert, Observations of normal modes for 84 recordings of the Alaskan Earthquake of 1964, March 28, *Geophysical Journal of the Royal Astronomical Society*, *27* (4), 393-446, 1972.

Dziewonski, A.M., and F. Gilbert, The effect of small, aspherical perturbations on travel times and a re-examination of the corrections for ellipticity, *Geophysical Journal of the Royal Astronomical Society*, *44*, 7-17, 1976.

Elsasser, W.M., Induction effects in terrestrial magnetism, I, theory, *Physics Reviews*, *67*, 106-116, 1946.

Engdahl, E.R., and L.E. Johnson, Differential PcP times and the radius of the core, *Geophysical Journal of the Royal Astronomical Society*, *39* (3), 435-456, 1974.

Ergin, K., Seismic evidence for a new layered structure of the Earth's core, *Journal of Geophysical Research*, *72*, 3669, 1967.

Garnero, E.J., and D.V. Helmberger, Travel Times of S and SKS: Implications for three-dimensional lower mantle structure beneath the central Pacific, *Journal of Geophysical Research*, *98*, 8225-8241, 1993.

Giardini, D., X.D. Li, and J.H. Woodhouse, Three-dimensional structure of the Earth from splitting in free-oscillation spectra, *Nature*, *325*, 405-411, 1987.

Glatzmaier, G., and P.H. Roberts, Intermediate Dynamo Models, *Journal of Geomagnetism and GeoElectricity*, *45*, 1605-1616, 1993.

Grand, S.P., Mantle shear structure beneath the Americas and surrounding oceans, *Journal of Geophysical Research*, *99* (B6), 11591-11621, 1994.

Gubbins, D., and P.H. Roberts, Magnetohydrodynamics of the Earth's core, in *Geomagnetism*, edited by J.A. Jacobs, pp. 1-183, Academic Press, London, 1987.

Gutenberg, B., and C.F. Richter, On Seismic Waves, *Gerlands Beitrage zur Geophysik*, *54*, 94-136, 1939.

Haddon, R.A.W., and J.R. Cleary, Evidence for scattering of seismic PKP waves near the mantle-core boundary, *Physics of the Earth and Planetary Interiors*, *8* (3), 211-234, 1974.

Hall, H.T., and V.R. Murthy, The early chemical history of the Earth: some critical elemental fractionations, *Earth and Planetary Science Letters*, *11* (2), 239-244, 1971.

Helffrich, G., and S. Sacks, Scatter and bias, differential PKP travel times and implications for mantle and core phenomena, *Geophysical Research Letters*, *21*, 2167-2170, 1994.

Huseby, E., and R. Madariaga, The origin of precursors to core waves, *Bulletin of the Seismological Society of America*, *61*, 429, 1970.

Jacobs, J.A., *Deep interior of the Earth*, Chapman and Hall, New York, 1992.

Jeanloz, R., and T.J. Ahrens, Equation of state of FeO and CaO, *Geophysical Journal of the Royal Astronomical Society*, *62* (3), 505-528, 1980.

Jeanloz, R., and H.R. Wenk, Convection and anisotropy of the inner core, *Geophysical Research Letters*, *15* (3), 72-75, 1988.

Jeffreys, H., The Times of the Core Waves (second paper), *Monthly Notices of the Royal Astronomical Society, Geophysics Supplement*, *4*, 594-615, 1939.

Jephcoat, A., and P. Olson, Is the inner core of the Earth pure iron?, *Nature*, *325* (6102), 332-335, 1987.

Johnson, L.R., Array measurements of P velocities in the lower mantle, *Bulletin of the Seismological Society of America*, *59* (2), 973-1008, 1969.

Julian, B.R., PKJKP, *Nature*, *235* (5337), 317-318, 1972.

Karato, S., Magnetic-field-induced preferred orientation of iron, *Science*, *262*, 1708-1711, 1993.

King, D.W., R.A.W. Haddon, and J.R. Cleary, Array analysis of precursors to PKiKP in the distance range 128° to 142°, *Geophysical Journal of the Royal Astronomical Society*, *37*, 157-173, 1974.

Knittle, E., and R. Jeanloz, High pressure metallization of FeO and implications for the Earth's core, *Geophysical Research Letters*, *13* (B), 1541-1544, 1986.

Knittle, E., and R. Jeanloz, Earth's core-mantle boundary: results of experiments at high pressures and temperatures, *Science*, *251* (5000), 1438-1443, 1991.

Kraft, A., H. Stiller, and H. Vollstaedt, The monosulfide solution in the Fe-Ni-S system: relationship to the Earth's core on the basis of experimental high-pressure investigations, *Physics of the Earth and Planetary Interiors*, *27* (4), 255-262, 1982.

Lehman, I., P', *Publications du Bureau Central Seismologique International: Series A*, *14* (3), 1936.

Lewis, J.S., Consequences of the prescence of sulphur in the core of the Earth, *Earth and Planetary Science Letters*, *11*, 130, 1971.

Li, X.D., D. Giardini, and J.H. Woodhouse, Large-scale three-dimensional even-degree structure of the Earth from splitting of long-period normal modes, *Journal of Geophysical Research*, *96* (B1), 551-577, 1991.

Li, X.D., and B. Romanowicz, Global Tomographic Model for the Mantle Obtained Using Non-Linear Asymptotic Coupling Theory (abstract), *EOS Transactions of the American Geophysical Union*, *75*, 71-72, 1994.

Masters, G., H. Bolton, and P. Shearer, Large-scale 3-dimensional structure of the mantle (abstract), *EOS Transactions of the American Geophysical Union*, *73*, 201, 1992.

Masters, G., and F. Gilbert, Structure of the inner core inferred from observations of its spheroidal shear modes, *Geophysical Research Letters*, *8*, 569-571, 1981.

Masters, T.G., Structure of the Earth: mantle and core, *Reviews of Geophysics*, *29*, 671-679, 1991.

Masters, T.G., and P.M. Shearer, Summary of seismological constraints on the structure of the Earth's core, *Journal of Geophysical Research*, *95* (B13), 21691-21695, 1990.

McFadden, P.L., and R.T. Merrill, History of Earth's magnetic field and possible connections to core-mantle boundary processes, *Journal of Geophysical Research*, *100*, 307-316, 1995.

McFadden, P.L., R.T. Merrill, and M.W. McElhinny, Nonlinear processes in the geodynamo: Paleomagnetic evidence, *Geophysical Journal of the Royal Astronomical Society*, *83*, 111-126, 1985.

Merrill, R.T., and P.L. McFadden, *The Earth's magnetic field; its history origin and planetary perspective*, Academic Press, New York, 1983.

Merrill, R.T., and P.L. McFadden, Dynamo Theory and Paleomagnetism, *Journal of Geophysical Research*, *100*, 317-326, 1995.

Michelini, A., and T.V. McEvilly, Seismological studies at Parkfield, I, simultaneous inversion for velocity structure and hypocenters using cubic B-splines parameterization, *Bulletin of the Seismological Society of America*, *81*, 524-552, 1991.

Morelli, A., and A.M. Dziewonski, Topography of the core-mantle boundary and lateral heterogeneity of the liquid core, *Nature*, *325*, 678-683, 1987.

Morelli, A., A.M. Dziewonski, and J.H. Woodhouse, Anisotropy of the inner core inferred from PKIKP travel times, *Geophysical Research Letters*, *13*, 1545-1548, 1986.

Murthy, V.R., and H.T. Hall, The chemical composition of the Earth's core; possibility of sulphur in the core, *Physics of the Earth and Planetary Interiors*, *2*, 276, 1970.

Parker, R. L., *Geophysical Inverse Theory*, Princeton University Press, New Jersey, 1994.

Phinney, R.A., and S.S. Alexander, P-wave diffraction theory and the structure of the core-mantle boundary, *Journal of Geophysical Research*, *71* (24), 5959-5975, 1966.

Poirier, J.P., *Introduction to the Physics of the Earth's Interior*, Cambridge University Press, New York, 1991.

Poupinet, G., R. Pillet, and A. Souriau, Possible heterogeneity of the Earth's core deduced from PKIKP travel times, *Nature*, *305*, 204-206, 1983.

Pulliam, R.J., and P.B. Stark, Bumps on the core-mantle boundary: are they facts or artifacts?, *Journal of Geophysical Research*, *98* (B2), 1943-1955, 1993.

Qamar, A., Revised velocities in the Earth's core, *Bulletin of the Seismological Society of America*, *63*, 1073, 1973.

Ringwood, A.E., Composition of the core and implication for the origin of the Earth, *Geochemical Journal*, *11* (3), 111-135, 1978.

Ritzwoller, M., G. Masters, and J.H. Woodhouse, Observations of anomalous splitting and their interpretation in terms of aspherical structure, *Journal of Geophysical Research*, *91*, 10203-10228, 1986.

Roberts, P.H., Origin of the main field; dynamics, in *Geomagnetism*, edited by J.A. Jacobs, pp. 185-249, Academic Press, London, 1987.

Roberts, P.H., and D. Gubbins, Origin of the main field; kinematics, in *Geomagnetism*, edited by J.A. Jacobs, pp. 185-249, Academic Press, London, 1987.

Rodgers, A., and J. Wahr, Inference of core-mantle boundary topography from ISC PcP and PKP traveltimes, *Geophysical Journal International*, *115* (3), 991-1011, 1993.

Shearer, P.M., Constraints on inner core anisotropy from PKP(DF) travel times, *Journal of Geophysical Research*, *99* (B10), 19647-19659, 1994.

Shearer, P.M., and K.M. Toy, PKP(BC) versus PKP(DF) differential travel times and aspherical structure in the Earth's inner core, *Journal of Geophysical Research*, *96*, 2233-2247, 1991.

Shearer, P.M., K.M. Toy, and J.A. Orcutt, Axi-symmetric Earth models and inner-core anisotropy, *Nature*, *333*, 228-232, 1988.

Somerville, M.R., and T.J. Ahrens, Shock compression of $KFeS_2$ and the question of potassium in the core, *Journal of Geophysical Research*, *85*, 7016, 1980.

Song, X., and D.V. Helmberger, Velocity structure near the inner core boundary from waveform modeling, *Journal of Geophysical Research*, *97* (B5), 6573-6586, 1992.

Song, X., and D.V. Helmberger, Anisotropy of Earth's inner core, *Geophysical Research Letters*, *20* (23), 2591-2594, 1993a.

Song, X., and D.V. Helmberger, Effect of velocity structure in D" on PKP phases, *Geophysical Research Letters*, *20* (4), 285-288, 1993b.

Song, X., and D.V. Helmberger, Depth dependance of inner core anisotropy, *EOS Transactions of the American Geophysical Union*, *75*, 71, 1994.

Souriau, and Souriau, Ellipticity and density at the inner core boundary from subcritical PKiKP and PcP data, *Geophysical Journal of the Royal Astronomical Society*, *98* (1), 39-54, 1989.

Stacey, F.D., *Physics of the Earth*, Brookfield Press, Brisbane, 1992.

Stixrude, L., and R.E. Cohen, High-pressure elasticity of iron and anisotropy of Earth's inner core, *Science*, *267*, 1972-1975, 1995.

Su, W.J., and A.M. Dziewonski, Inner Core Anisotropy in Three Dimensions (abstract), *EOS Transactions of the American Geophysical Union*, *75*, 71, 1994.

Tromp, J., Support for anisotropy of the Earth's inner core from free oscillations, *Nature*, *366* (6456), 678-681, 1993.

Vinnik, L., B. Romanowicz, and L. Breger, Anisotropy in the center of the inner core, *Geophysical Research Letters*, *21* (16), 1671-1674, 1994.

Widmer, R., G. Masters, and F. Gilbert, Observably split multiplets; data analysis and interpretation in terms of large-scale aspherical structure, *Geophysical Journal International*, *111*, 559-576, 1992.

Woodhouse, J.H., D. Giardini, and X.D. Li, Evidence for inner core anisotropy from splitting in free oscillation data, *Geophysical Research Letters*, *13*, 1549-1552, 1986.

Woodward, R.L., and G. Masters, Lower-mantle structure from ScS-S differential travel times, *Nature*, *352* (6332), 231-233, 1991.

Wysession, M.E., L. Bartko, and J.B. Wilson, Mapping the lowermost mantle using core-reflected shear waves, *Journal of Geophysical Research*, *99*, 13667-13684, 1994.

Wysession, M.E., and E.A. Okal, Regional analysis of D" velocities from the ray parameters of diffracted P profiles, *Geophysical Research Letters*, *16* (12), 1417-1420, 1989.

Wysession, M.E., E.A. Okal, and C.R. Bina, The structure of the core-mantle boundary from diffracted waves, *Journal of Geophysical Research*, *97* (B6), 8749-8764, 1992.

Appendix A: How Good is PREM?

A.1 Comparison of PREM to differential travel time observations

The core model put forth by PREM [*Dziewonski and Anderson*, 1981] is not a sufficient model for the data presented here. The data that we will be presenting have all been drawn from the GDSN/GSN networks and represent a combination of data distributed by the IRIS DMC as part of their FARM and data distributed on CDROM by the NEIC. Wherever possible, the data have been converted to a common instrument response (in this case DWWSSN short period) if they were from broadband recordings in order to allow for comparison with the GDSN short period data that was collected from the FARM prior to 1988 and from the NEIC from 1980-1987. Regional array data, although part of our larger dataset, have been removed for this comparison, as have any data that may have been effected by the anisotropy of the inner core. As was discussed in Chapter 2, an angle between the direction of the P'_{DF} ray at its turning point and the symmetry axis of the anisotropy (ξ) can be defined. By removing all data (either P'_{AB}-P'_{DF} or P'_{BC}-P'_{DF}) with $\xi < 40°$, the effects of the inner core can be reduced. This is the procedure that we have followed here. As was the case in Chapter 2 and Chapter 3, no effort was made to try to correct the data for any "known" problems except for ellipticity. The results are summarized in Figures A–1 through A–3 and are discussed briefly below. Our interpretation of the residuals in our dataset assumes no lateral variations exist in the P-wave velocity of the liquid outer core. For a reference spherical earth model, however, one could modify the outer core, especially near the inner core boundary.

In Figure A–1 (a)-(c), the residuals in our dataset (with respect to PREM) are shown plotted as a function of distance for the P'_{AB}–P'_{DF}, P'_{BC}–P'_{DF}, and P'_{AB}–P'_{BC} phase pairs separately. The data are the blue dots and the mean and standard error in the estimate of the mean. As was discussed in Chapter 2 and Chapter 3, the P'_{BC}–P'_{DF} phase pair is most strongly effected by structure in the inner core, while the P'_{AB}–P'_{BC} phase pair will most

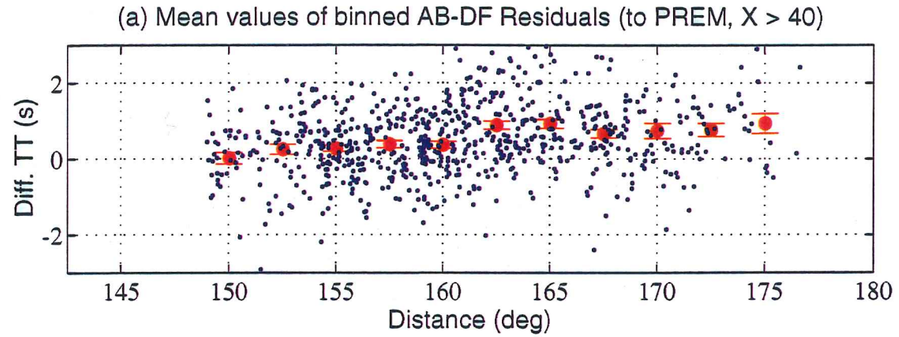

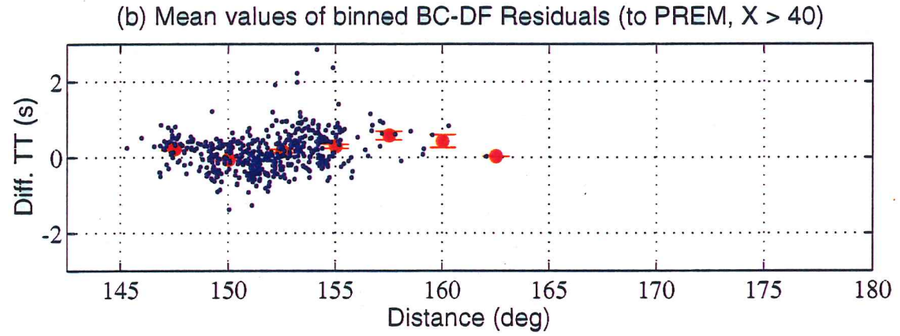

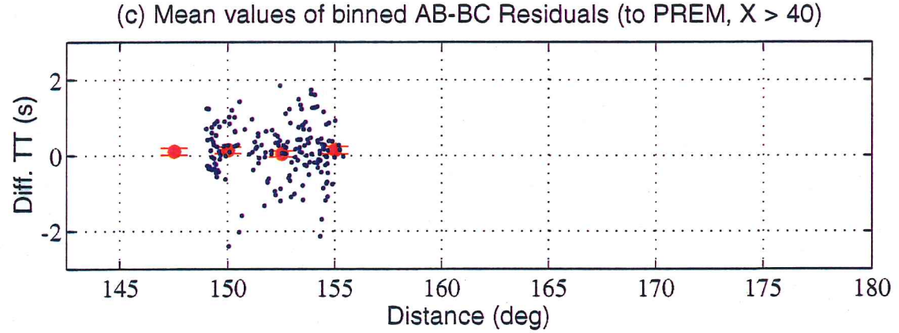

Figure A-1: A plot showing the mean values and standard errors in the estimate of the mean values for the residuals (with respect to PREM) of the (a) P'_{AB}–P'_{DF}, (b) P'_{AB}–P'_{DF} and (c) P'_{AB}–P'_{DF} times as a function of distance. The data are plotted as blue dots, the mean values as red dots, and the error bars represent plus and minus one standard error. This figure is discussed rather extensively in the text.

strongly show the effects of lower mantle and D" structure. The P'_{AB}–P'_{DF} phase pair should show a combination of both lower mantle and inner core structure, with the structure in the D" region perhaps being the dominant effect in most cases. Several features are noticeable in this figure. First, and foremost, the P'_{AB}–P'_{BC} times show no noticeable trend over the distance range that they are observed in (148° to 155°), suggesting that, in the global sense, the PREM D" model is adequate throughout. The scatter in the data also appears to increase with distance, suggesting that the scatter in these times is due to the sensitivity of this phase pair to differences in velocity structure of D" near the P'_{AB} interaction point. Over this same distance range, however, there is a pronounced concave upward bend in the observed P'_{BC}-P'_{DF} times. These times are distinctly positive at 147°, decrease to zero at 150°, and then increase again as one approaches 155°. The scatter in the data is relatively constant about this sinusoidal distribution of mean values, suggesting that this scatter could be due to structure in the inner core (since it doesn't change with distance). The distribution of the mean values suggests that the PREM inner-core model is too slow near the ICB and is too slow as one moves deeper than about 150 km depth in the IC. This is supported quite dramatically by the P'_{AB}-P'_{DF} times, which start out at a nearly zero value at 150° and grow steadily more positive (in an average sense) as distance increases. While these do suggest a problem with the inner-core model of PREM being to slow overall (giving rise to, on average, positive residuals at distances either less than or greater than 150°), it may be that D" is too fast in the PREM model, but the P'_{AB}-P'_{BC} times seem to contradict this.

Figure A–2 (a)-(c) shows the same data plotted versus ray angle (ξ). Again the three phase pairs have been separated out into three separate plots. As is readily apparent, the scatter of their P'_{AB}-P'_{DF} times about their mean values is nearly twice the scatter of the P'_{BC}-P'_{DF} times about their mean values at a given value of ξ. This is really just a restatement of an observation that was made in Chapter 2. Of particular interest, however, is the third plot (c). Here the predominant trend in residuals with respect to PREM that exists in the P'_{AB}-P'_{DF} and P'_{BC}-P'_{DF} times (of increasing residuals with increasing ξ) is completely

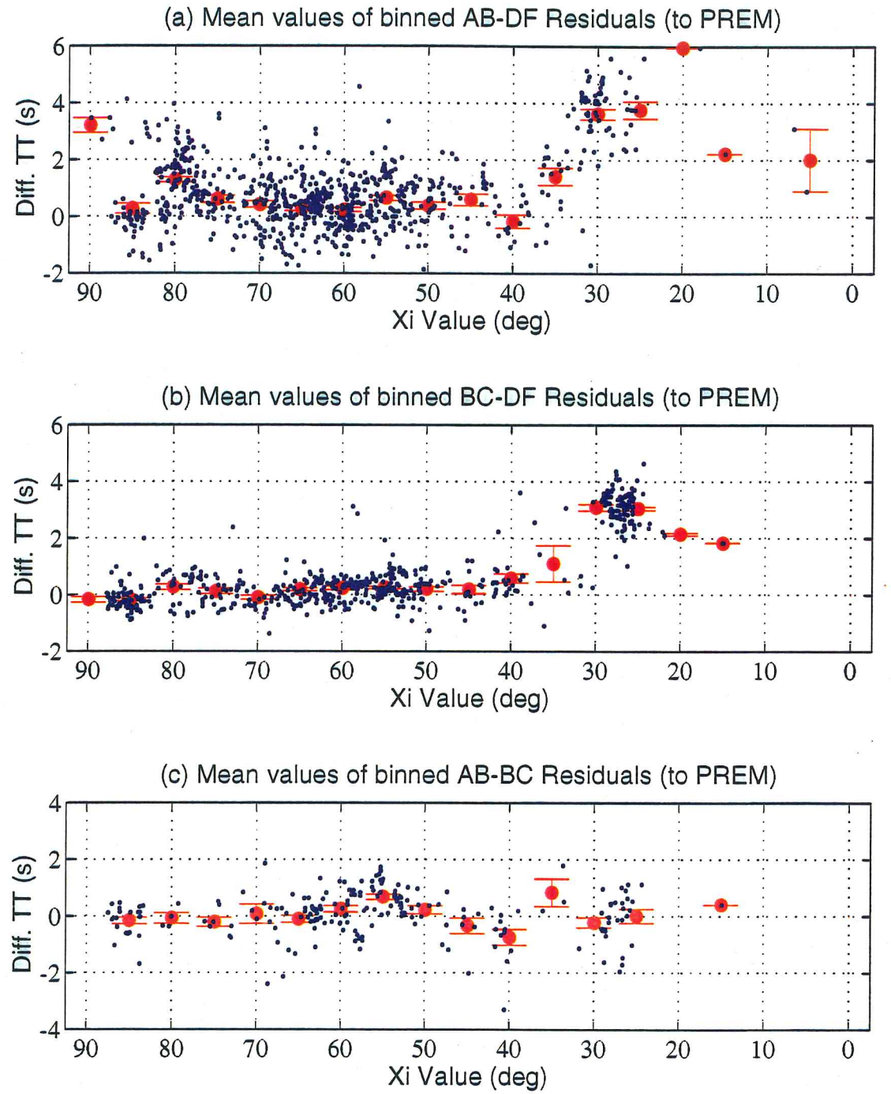

Figure A-2: The same data as plotted in Figure A-1, plotted versus the angle (ξ) that the P'_{DF} ray makes with respect to the spin axis of the earth at its turning point. In (c), the angle (ξ) is the angle of the corresponding P'_{DF} ray (i.e. the P'_{DF} ray that is from the same event-station pair as the P'_{AB} and P'_{BC} rays). Of particular interest is the lack of residual in (c) and the difference in scatter between (a) and (b).

missing. The residuals in P'_{AB}-P'_{BC} times with respect to both distance and ξ are essentially zero (there is no systematic variation). Again, this suggests that the signal observed in the P'_{AB}-P'_{DF} and P'_{BC}-P'_{DF} times is due to inner core anisotropy and not to structure in the outer core (which should effect the P'_{BC} rays at their turning point or near the poles nearly as strongly as the P'_{BC} rays are effected.

Figure A–3 (a)-(g) is presented as a brief summary of the histograms of the dataset used in Chapter 2. This figure is fairly self explanatory. Of particular interest are panels (d) and (e), which most clearly show the effects of anisotropy on these phases. Panels (c) and (f) are presented to show that the residuals to our axisymmetric model are nearly gaussian.

In Conclusion: The PREM core model needs some significant revisions. Based on the data shown here, the PREM model fails to fit the average values of PKP differential travel times at great distances. Based on the similarity of the size of the anomalous mean values, it seems that the most likely explanation is that, overall, the PREM inner core is too slow, although a PREM lower mantle/D" region that is too fast may be able to account for the residuals that we observe.

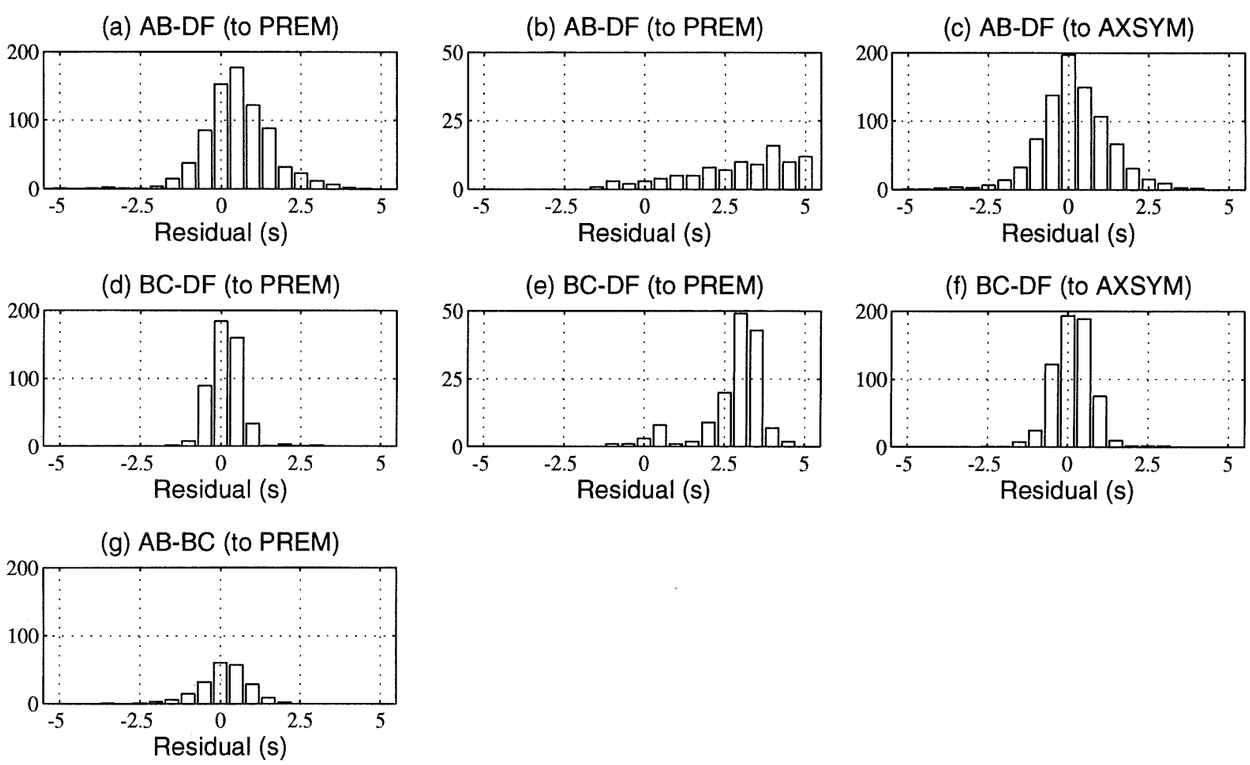

Figure A-3: The histograms of the residuals with respect to PREM of (a) and (b) $P'_{AB} - P'_{DF}$ times with $\xi > 40°$ and $\xi < 40°$, respectively; (d) and (e), the same as (a) and (b) but for $P'_{BC} - P'_{DF}$ times; (c) and (f), residuals with respect to our AXSYM inner core anisotropy model for $P'_{AB} - P'_{DF}$ and $P'_{BC} - P'_{DF}$ times respectively; and (g) the residuals with respect to PREM of our $P'_{AB} - P'_{BC}$ times

Thomas J. McSweeney recieved his Bachelor of Science in Earth Science from the University of Notre Dame (Notre Dame, IN), in May of 1987. He went on to recieve a Masters of Science Degree in Seismology from the University of Alaska, Fairbanks in September 1989. Since that time, he has been continuing his studies in Seismology here at the University of Washington in Seattle.